Cellular/Molecular

Deletion of *Stim1* in Hypothalamic Arcuate Nucleus Kiss1 Neurons Potentiates Synchronous GCaMP Activity and Protects against Diet-Induced Obesity

Jian Qiu,[1] Todd L. Stincic,[1] Martha A. Bosch,[1] Ashley M. Connors,[1] Stefanie Kaech Petrie,[2] Oline K. Rønnekleiv,[1,3] and Martin J. Kelly[1,3]

[1]Department of Chemical Physiology and Biochemistry, Oregon Health and Science University, Portland, Oregon 97239, [2]Jungers Center for Neurosciences Research, Oregon Health and Science University, Portland, Oregon 97239, and [3]Division of Neuroscience, Oregon National Primate Research Center, Oregon Health and Science University, Beaverton, Oregon 97006

Kisspeptin (Kiss1) neurons are essential for reproduction, but their role in the control of energy balance and other homeostatic functions remains unclear. High-frequency firing of hypothalamic arcuate Kiss1 ($Kiss1^{ARH}$) neurons releases kisspeptin into the median eminence, and neurokinin B (NKB) and dynorphin onto neighboring $Kiss1^{ARH}$ neurons to generate a slow EPSP mediated by TRPC5 channels that entrains intermittent, synchronous firing of $Kiss1^{ARH}$ neurons. High-frequency optogenetic stimulation of $Kiss1^{ARH}$ neurons also releases glutamate to excite the anorexigenic proopiomelanocortin (POMC) neurons and inhibit the orexigenic neuropeptide Y/agouti-related peptide (AgRP) neurons via metabotropic glutamate receptors. At the molecular level, the endoplasmic reticulum (ER) calcium-sensing protein stromal interaction molecule 1 (STIM1) is critically involved in the regulation of neuronal Ca^{2+} signaling and neuronal excitability through its interaction with plasma membrane (PM) calcium (e.g., TRPC) channels. Therefore, we hypothesized that deletion of *Stim1* in $Kiss1^{ARH}$ neurons would increase neuronal excitability and their synchronous firing, which ultimately would affect energy homeostasis. Using optogenetics in combination with whole-cell recording and GCaMP6 imaging in slices, we discovered that deletion of *Stim1* in Kiss1 neurons significantly increased the amplitude and duration of the slow EPSP and augmented synchronous $[Ca^{2+}]$i oscillations in $Kiss1^{ARH}$ neurons. Deletion of *Stim1* in $Kiss1^{ARH}$ neurons amplified the actions of NKB and protected ovariectomized female mice from developing obesity and glucose intolerance with high-fat dieting (HFD). Therefore, STIM1 appears to play a critical role in regulating synchronous firing of $Kiss1^{ARH}$ neurons, which ultimately affects the coordination between energy homeostasis and reproduction.

Key words: calcium; KNDy neurons; neurokinin B; slow EPSP; stromal interaction molecule 1; TRPC5 channel

Significance Statement

Hypothalamic arcuate kisspeptin ($Kiss1^{ARH}$) neurons are essential for stimulating the pulsatile release of gonadotropin-releasing hormone (GnRH) and maintaining fertility. However, $Kiss1^{ARH}$ neurons appear to be a key player in coordinating energy balance with reproduction. The regulation of calcium channels and hence calcium signaling is critically dependent on the endoplasmic reticulum (ER) calcium-sensing protein stromal interaction molecule 1 (STIM1), which interacts with the plasma membrane (PM) calcium channels. We have conditionally deleted *Stim1* in $Kiss1^{ARH}$ neurons and found that it significantly increased the excitability of $Kiss1^{ARH}$ neurons and protected ovariectomized female mice from developing obesity and glucose intolerance with high-fat dieting (HFD).

Received Mar. 15, 2021; revised June 29, 2021; accepted Oct. 7, 2021.

Author contributions: J.Q., T.L.S., M.A.B., A.M.C., O.K.R., and M.J.K. designed research; J.Q., T.L.S., M.A.B., and A.M.C. performed research; S.K.P., O.K.R., and M.J.K. contributed unpublished reagents/analytic tools; J.Q., T.L.S., M.A.B., A.M.C., O.K.R., and M.J.K. analyzed data; J.Q., O.K.R., and M.J.K. wrote the first draft of the paper; J.Q., T.L.S., M.A.B., S.K.P., O.K.R., and M.J.K. edited the paper; J.Q., O.K.R., and M.J.K. wrote the paper.

This work was supported by National Institutes of Health Grants R01-NS043330 (to O.K.R.), R01-NS038809 (to M.J.K.), and R01-DK068098 (to O.K.R. and M.J.K.). Confocal microscopy was supported by the NIH Grant P30 NS061800 (PI, S. Aicher). We thank Mr. Daniel Johnson for his technical support.

The authors declare no competing financial interests.

Correspondence should be addressed to Jian Qiu at qiuj@ohsu.edu or Martin J. Kelly at kellym@ohsu.edu.

https://doi.org/10.1523/JNEUROSCI.0622-21.2021

Introduction

Nutrition and reproduction are inextricably linked across all mammalian species, i.e., high circulating concentrations of 17β-estradiol (E2) during the late follicular phase of the reproductive cycle correlate with reduced food intake (Czaja, 1978; Asarian and Geary, 2006; Roepke et al., 2010). However, we are just beginning to understand the central mechanisms by which E2 feedback coordinates reproduction and energy balance (Castellano and Tena-Sempere, 2013; Nestor et al., 2014; Navarro, 2020). Kisspeptin neurons in the hypothalamic arcuate nucleus

(Kiss1^{ARH} neurons) appear to be critical for coordinating these two homeostatic processes. First, Kiss1 and its G-protein-coupled receptor (GPR54) are essential for pubertal development and reproductive function (Kuohung and Kaiser, 2006). Mutations in Kiss1 or GPR54 cause hypogonadotropic hypogonadism in humans (De Roux et al., 2003; Seminara et al., 2003; Topaloglu et al., 2012), and deletion of Kiss1 or GPR54 causes defective sexual development and reproductive failure in mice (Seminara et al., 2003; d'Anglemont de Tassigny et al., 2007). These effects on fertility are directly dependent on Kiss1/GPR54 signaling in gonadotropin-releasing hormone (GnRH) neurons (Han et al., 2005; Pielecka-Fortuna et al., 2008; Zhang et al., 2008). Moreover, Kiss1 signaling appears to be also important for normal metabolism and glucose homeostasis. GPR54 deletion in female, but not male, mice causes severe obesity, reduced metabolism, glucose intolerance and hyperleptinemia (Tolson et al., 2014, 2019). Also, Kiss1^{ARH} neurons are directly depolarized/excited by leptin (Qiu et al., 2011) and insulin (Qiu et al., 2014), so they are quite possibly key neurons involved in conveying metabolic information to GnRH neurons.

High-frequency optogenetic stimulation of Kiss1^{ARH} neurons expressing channelrhodopsin (ChR2) generates pulsatile release of luteinizing hormone (LH; Clarkson et al., 2017). Kiss1^{ARH} neurons co-express neurokinin B (NKB) and dynorphin (Goodman et al., 2007; Navarro et al., 2009) and high-frequency firing (10–20 Hz) of these neurons co-releases NKB and dynorphin to coordinate the synchronous firing of the whole population of Kiss1^{ARH} neurons (Qiu et al., 2016). NKB binds to tachykinin 3 receptor (TacR3) in neighboring Kiss1^{ARH} neurons to activate canonical transient receptor potential 5 (TRPC5) channels to cause a robust depolarization (slow EPSP), whereas co-released dynorphin feeds back to bind to presynaptic κ-opioid receptors to limit the release of NKB to discrete bursts of activity (Qiu et al., 2016). The co-release of the two peptide neurotransmitters coordinates the synchronous firing of Kiss1^{ARH} neurons that drives the pulsatile release of GnRH into the median eminence (Qiu et al., 2016; Clarkson et al., 2017).

The activity of TRPC channels is modulated by stromal interaction molecule 1 (STIM1), which is localized to the endoplasmic reticulum (ER) membrane of cells, and its N-terminal domain contains an EF-hand that senses changes in ER calcium concentrations and maintains intracellular Ca^{2+} homeostasis through store-operated Ca^{2+} entry (SOCE; Salido et al., 2011). Upon depletion of ER Ca^{2+}, STIM1 oligomerizes and then interacts with plasma membrane (PM) calcium (TRPC) channels (Yuan et al., 2007; Salido et al., 2011). Phosphorylation of STIM1 is required for oligomerization, and E2 inhibits the phosphorylation of STIM1 and its interaction with PM Orai and TRPC channels and hence SOCE (Yuan et al., 2007; Salido et al., 2011). Under normal physiological conditions, TRPC5 channels are coupled to PM receptors (Qiu et al., 2010, 2014; Gao et al., 2017), but in cellular stressed states (e.g., inflammation, obesity), TRPC5 channels may associate with STIM1 to replete ER Ca^{2+} stores (Birnbaumer, 2009; Qiu et al., 2018b). E2 maintains the excitatory effects of insulin in proopiomelanocortin (POMC) neurons, mediated by TRPC5 channel opening, by downregulating *Stim1* expression in the ARH, thereby protecting against insulin resistance in obese females (Qiu et al., 2018b). E2 also downregulates *Stim1* expression in the ARH of female guinea pigs, indicating that E2's effects maybe universal (Qiu et al., 2018b). Therefore, we hypothesized that deletion of *Stim1* in Kiss1^{ARH} neurons would augment TacR3 mediated depolarization via TRPC5 channels to ultimately drive synchronous firing of the "pulse-generator" Kiss1^{ARH} neurons.

Materials and Methods

Animals

All animal procedures were conducted at Oregon Health and Science University (OHSU) according to the National Institutes of Health *Guide for the Care and Use of Laboratory Animals* and with approval from the OHSU Animal Care and Use Committee.

We used female mice in all of the experiments. *Kiss1*$^{Cre:GFP}$ (v2) mice (Richard D. Palmiter; University of Washington; Padilla et al., 2018) were housed under constant temperature (21–23°C) and 12/12 h light/dark cycle schedule (lights on at 6 A.M. and lights off at 6 P.M.), with free access to food (Lab Diets 5L0D) and water. *Kiss1*$^{Cre:GFP}$ mice were used for viral injection to express ChR2 or GCaMP6s in Kiss1^{ARH} neurons or they were crossed with homozygous *Ai32* mice (RRID:IMSR_JAX:024109, C57BL/6 background) purchased from The Jackson Laboratory. These *Ai32* mice carry the ChR2 (H134R)–EYFP gene in their Gt(ROSA)26Sor locus (Madisen et al., 2012). The gene is separated from its CAG promoter by a loxP-flanked transcriptional STOP cassette, allowing its expression in a Cre-dependent manner. To test for this, we dispersed and harvested EYFP neurons in the ARH from *Kiss1*$^{Cre:GFP}$::*Ai32* females and used single-cell RT-PCR (scRT-PCR) to determine *Kiss1* mRNA expression as described below and according to previous published methods (Bosch et al., 2013). Data from 126 ARH^{EYFP} neurons from 6 *Kiss1*$^{Cre:GFP}$::*Ai32* females documented that 99% of the EYFP neurons expressed *Kiss1*.

To generate mice with conditional knock-out of *Stim1* in Kiss1 neurons (*Stim1*^{kko}), we first crossed *Kiss1*$^{Cre/+}$ (v2) males (Padilla et al., 2018) with *Stim1*$^{fl/fl}$ females (The Jackson Laboratory stock #023350, RRID:IMSR_JAX:023350; Oh-hora et al., 2008). This cross knocks out *Stim1* through excising exon 2 (Oh-hora et al., 2008) of the floxed *Stim1* gene in cells in which Cre is expressed under the control of a promoter specific for the expression of *Kiss1* (Padilla et al., 2018; Qiu et al., 2018a). The F1 mice produced were *Kiss1*$^{Cre/+}$::*Stim1*$^{+/lox}$ and *Stim1*$^{+/lox}$. The F2 mice were generated by crossing these *Kiss1*$^{Cre/+}$::*Stim1*$^{+/lox}$ males with *Stim1*$^{lox/lox}$ females. Approximately 25% of the offspring were *Kiss1*$^{Cre/+}$::*Stim1*$^{lox/lox}$ such that *Stim1* was deleted in Kiss1 cells (*Stim1*^{kko}), and all the *Stim1* knock-out mice were seen at the expected frequency and viable throughout adulthood. We used *Kiss1*$^{Cre/+}$ mice as controls. To increase the yield of *Stim1* knock-out mice, we crossed *Kiss1*$^{Cre/+}$::*Stim1*$^{lox/lox}$ males with *Stim1* $^{lox/lox}$ females. We maintained not only this strain but also the *Kiss1*$^{Cre/+}$ strain at the same time. Genotypes for *Stim1* were determined using forward primer JAX#18 885 (5'-CGA TGG TCT CAC GGT CTC TA-3') and reverse primer JAX#18 886 (5'-GCT CTG CTG ACC TGG AAC TA-3'), which distinguished between *lox/lox*, *lox/+*, and +/+ genotypes. *Cre* genotypes were determined using forward primer 5'-GCG GTC TGG CAG TAA AAA CTA TC-3' and reverse primer 5'-TTC CAT GAG TGA ACG AAC CTG G-3', which distinguished between carriers and non-carriers of the *Cre* allele.

Puberty onset and estrous cyclicity

To determine whether deleting *Stim1* in Kiss1-expressing neurons might impact fertility, we evaluated female *Stim1*^{kko} mice and wild-type (WT) female littermates for pubertal onset and estrous cyclicity. For breeding, male and female mice were mated at 1:1, and the number of pups per litter was counted. The *Stim1*^{kko} mice showed similar fecundity as control mice. Puberty onset in females was assessed by monitoring for vaginal opening daily between 9 and 10 A.M. starting at three weeks of age. For estrous cycle studies, *Stim1*^{kko} and *Kiss1*$^{Cre:GFP}$ female mice were group housed and were habituated to handling for at least one week by the same investigator before estrous cycle monitoring. Vaginal lavage was performed daily for 13 consecutive days between 9 and 10 A.M. Cytology was evaluated using a light microscope and scored as diestrus, proestrus or estrus as previously described (Qiu et al., 2018a). The

Number of estrous and diestrous days were counted for each animal and used for statistical analysis (Mann–Whitney *U* test).

Gonadectomy

At least 7 d before each experiment, ovaries were removed as described previously while under inhalant isofluorane anesthesia (Piramal Enterprises Limited; Qiu et al., 2018a). Each mouse received analgesia (carprofen; 5 mg/kg, s.c.) immediately after a surgery for relief of postoperative pain.

Metabolic studies

For the metabolic studies, *Stim1*^{kko} and *Kiss1* littermate control females were ovariectomized at two to four months of age and put on a high-fat diet (HFD; 45% kcal from fat; Research Diets; D12451) for eight weeks. Mice were group housed (because of COVID-19 restrictions) and individually weighed every week. The evening before the glucose tolerance test (GTT), all mice were assessed for body composition (fat and lean mass) using an EchoMRI 4-in-1-500 Body Composition Analyzer.

For GTT, age matched *Kiss1*^{Cre} and *Stim1*^{kko} mice were fasted overnight for 15 h, and baseline glucose levels measured with the aid of an Accu-Check Advantage blood glucose meter (Roche) using blood collected from the tail vein. All mice were then injected intraperitoneally with glucose (1 mg/g lean mass as determined by EchoMRI) in sterile PBS and blood glucose levels were measured 15, 30, 60, 90, and 120 min after injection. The glucose clearance (area under the curve; AUC) was calculated based on the glucose baseline levels at 0 min (Ayala et al., 2010).

AAV delivery to Kiss1$^{Cre:GFP}$ *and Stim1*^{kko} *mice*

Fourteen to 21 d before each experiment, *Kiss1*$^{Cre:GFP}$ mice or *Stim1*^{kko} mice (>60 d old) received bilateral ARH injections of a Cre-dependent adeno-associated viral (AAV; serotype 1) vector encoding ChR2-mCherry (AAV1-Ef1a-DIO-ChR2: mCherry) or ChR2-YFP (AAV1-Ef1a-DIO-ChR2:YFP, Stephanie L. Padilla; University of Washington) or GCaMP6s (AAV9-Syn-Flex-GCaMP6s-WPRE-SV40; Addgene, #100845-AAV9). Using aseptic techniques, anesthetized female mice (1.5% isoflurane/O_2) received a medial skin incision to expose the surface of the skull. The glass pipette (Drummond Scientific #3-000-203-G/X) with a beveled tip (diameter = 45 μm) was filled with mineral oil, loaded with an aliquot of AAV using a Nanoject II (Drummond Scientific). ARH injection coordinates were anteroposterior (AP): −1.20 mm, mediolateral (ML): ± 0.30 mm, dorsoventral (DL): −5.80 mm (surface of brain z = 0.0 mm); 500 nl of the AAV (2.0×10^{12} particles/ml) was injected (100 nl/min) into each position, left in place for 10 min postinjection, then the pipette was slowly removed from the brain. The skin incision was closed using skin adhesive, and each mouse received analgesia (carprofen; 5 mg/kg) for 2 d postoperation.

Electrophysiology

Coronal brain slices (250 µm) containing the ARH from gonadectomized females were prepared as previously described (Qiu et al., 2003). Whole-cell, patch recordings were performed in voltage clamp and current clamp using an Olympus BX51W1 upright microscope equipped with video-enhanced, infrared-differential interference contrast (IR-DIC) and an Exfo X-Cite 120 Series fluorescence light source. Electrodes were fabricated from borosilicate glass (1.5-mm outer diameter; World Precision Instruments) and filled with a normal internal solution: 128 mM potassium gluconate, 10 mM NaCl, 1 mM $MgCl_2$, 11 mM EGTA, 10 mM HEPES, 3 mM ATP, and 0.25 mM GTP (pH was adjusted to 7.3–7.4 with 1N KOH, 290–300 mOsm). Pipette resistances ranged from 3 to 5 MΩ. In whole cell configuration, access resistance was <20 MΩ; access resistance was 80% compensated. For some experiments measuring the ramp current–voltage (I–V) relationship, K^+-gluconate in the normal internal solution was replaced with Cs^+-gluconate (pH 7.35 with CsOH), and the extracellular solution contained Na^+, K^+, I_h (HCN), Ca^{2+}, and $GABA_A$ channel blockers (126 mM NaCl, 5 mM 4-aminopyridine, 2.5 mM KCl, 1.2 mM $MgCl_2$, 2 mM CsCl, 1.4 mM $CaCl_2$, 1 mM $CoCl_2$, 0.01 mM nifedipine, 20 mM HEPES, 8 mM NaOH, 10 mM glucose, 0.001 mM tetrodotoxin (TTX), and 0.1 mM picrotoxin). The slope conductance was measured from −40 to −20 mV in the optimum range for detecting TRPC5 channel activity (Blair et al., 2009). For optogenetic stimulation, a light-induced response was evoked using a light-emitting diode (LED) 470-nm blue light source controlled by a variable 2A driver (ThorLabs) with the light path delivered directly through an Olympus 40 × water-immersion lens. High fidelity response to light (470 nm) stimulation of Kiss1^{ARH}::ChR2-mCherry expressing neurons was observed, and both evoked inward currents (in voltage clamp, V_{hold} = −60 mV) or depolarization (in current clamp) were measured. To characterize action potential (AP) properties, current-clamp recordings were obtained in the presence of antagonists of ionotropic glutamate and GABA receptors (50 μM D-APV, 10 μM CNQX, and 100 μM picrotoxin). The membrane potential of neurons was subsequently maintained around −70 mV by direct current injection. The excitability of neurons was assessed by injecting depolarizing currents (1 s steps, 5 pA increments). The first current step to display an AP was defined as the rheobase, and the first spike was analyzed in detail. AP properties were analyzed using Clampfit 11.2 software. Full-width at half-maximum (FWHM) of the AP, and afterhyperpolarization (AHP) time and amplitude were measured relative to threshold. Electrophysiological signals were amplified with an Axopatch 200A and digitized with Digidata 1322A (Molecular Devices), and the data were analyzed using p-Clamp software (RRID:SCR_011323, version 9.2, Molecular Devices). The amplitude of the slow EPSP was measured after low pass filtering to eliminate the barrage of APs riding on the depolarization. The liquid junction potential was corrected for all data analysis.

Calcium imaging

For calcium imaging, brain slices were placed in a RC-22C slide recording chamber (Harvard/Warner Instruments) and imaged on an inverted Nikon TiE microscope equipped with a Yokogawa CSU-W1 spinning disk confocal head, integrated under NIS Elements v4.20 (Nikon). The preparation, kept at 32°C via a cage incubator (Okolab), was continuously perfused with oxygenated artificial CSF (aCSF) at a flow rate of 1.25 ml/min. Images were acquired on a Zyla v5.5 sCMOS camera (Andor) at 0.5 Hz. frame-rate, through an 10 × (NA 0.45) or 20 × (NA 0.75) objective, combining 488 nm laser excitation with 500- to 550-nm emission collection. A single focal plane (*z*-axis) was maintained using the Nikon Perfect Focus System. Minor tissue drift in the x-*y*-axis was corrected using NIS Elements. Imaging displaying major drift were excluded from final analysis. Changes in Kiss1^{ARH} neuron Ca^{2+} levels were measured in regions of interest (ROIs) comprising the GCaMP6s-positive cell bodies. In all recordings, background fluorescence measured in an ROI drawn on nearby tissue was subtracted from every ROI. $[Ca^{2+}]_i$ variations after drug applications were assessed as changes in fluorescence signals over baseline ($\Delta F/F_0$). To normalize the fluorescence value of each cell, we first separated experimental trials into two parts: a baseline period (2 min) corresponding to all the frames recorded before addition of drugs, and a stimulus period, after the onset of the drug (such as bath-applied senktide) application and lasting several minutes. Next, for each ROI we calculated $\Delta F/F_0$ for each frame (t), where $\Delta F/F_0$ equals $(F_{(t)} - F_0)/F_0$, and F_0 was the mean fluorescence value for that ROI for all frames in the baseline period for that trial. The AUC was calculated over the time periods of 2 min before and 18 min after drug application. Maximal peak reached after drug application was also measured and used in quantitative analysis. Data were averaged across all Kiss1^{ARH} neurons in a slice (two slices per animal), which were used as the statistical unit over a minimum of three animals per condition.

scRT-PCR

Coronal brain sections from the ARH of three female *Stim1*^{kko} and three *Kiss1*$^{Cre:GFP}$*::Ai32* mice were prepared for electrophysiology and scRT-PCR. The 3–4 slices obtained were divided between electrophysiological recording experiments and single-cell harvesting. Single-cell dispersion and harvesting was performed as described previously with some modifcations as described below (Bosch et al., 2013; Zhang et al., 2013b). Briefly, the ARH was dissected and digested in papain (7 mg/ml in aCSF, Sigma-Aldrich). Gentle trituration using varying sizes of flame polished Pasteur pipets were used to disperse the cells and then they were plated

Table 1. Primer table

Gene name (encodes for)	Accession number	Primer location (nt)	Product length (bp)	Annealing temperature (°C)	Efficiency slope	r^2	%
Kiss1 (Kiss1)[a,b]	NM_178260	64–80 (exon 1) 167–183 (exon 2)	120	57[a], 60[b]	−3.410	0.989	97
Stim1 (STIM1)[a]	NM_009287	797–816 (exon 2) 981–1000 (exon 3)	204	59			
Stim1 (STIM1)[b]	NM_009287	821–839 (exon 2) 937–955 (exon 3)	135	60	−3.311	0.977	100
Stim2 (STIM2)	NM_001363348	620–638 (exon 2) 773–791 (exon 4)	172	59			
Stim2 (STIM2)[b]	NM_001363348	1784–1803 (exon 11) 1895–1914 (exon 12)	131	60	−3.439	0.993	95
Gapdh (GAPDH)[b]	NM_008084	689–706 (exon 4) 764–781 (exon 5)	93	60	−3.352	0.998	99
Trpc4 (TRPC4)[a,b]	NM_016984	1888–1907 (exon 6) 1984–2003 (exon 7)	116	60	−3.318	0.940	100
Trpc5 (TRPC5)[a]	NM_009428	2206–2227 (exon 6) 2315–2336 (exon 7)	131	63			
Trpc5 (TRPC5)[b]	NM_009428	734–753 (exon 2) 832–851 (exon 3)	118	60	−3.161	0.953	100

[a]primers for scRT-PCR.
[b]primers for qPCR.

onto a glass bottom dish. A constant flow of oxygenated aCSF (125 mM NaCl, 5 mM KCl, 1.44 mM NaH_2PO_4, 5 mM HEPES, 10 mM D-glucose, 26 mM $NaHCO_3$, 2 mM $MgSO_4.7H_2O$, and 2 mM $CaCl_2$) was applied to the dish to keep the cells healthy and to clear debris. Fluorescent neurons were visualized under an inverted microscope. The Xenoworks Microinjection system (Sutter Instruments) was used to manipulate a 10 µm tip size glass capillary tube to approach single neurons, apply gently suction and harvest single cells or pools of 10 cells into a siliconized tube containing a solution of 1× Invitrogen Superscript III Buffer (LifeTech), 15U of RNasin (Promega), 10 mM of dithiothreitol (DTT) and diethylpyrocarbonate (DEPC)-treated water in a total of 5 µl for single cells or 8 µl for pools of 10 cells. Corresponding controls were collected at the same time including single neurons (processed without reverse transcriptase) and aCSF from the surrounding area. Hypothalamic tissue RNA was also processed with and without reverse transcriptase. First strand cDNA synthesis was performed on single cells, pools of cells and controls in a 20 µl (single cells) or 25 µl (10 cell pools) volume containing a final concentration of 1× Invitrogen Superscript III Buffer, 30 U of RNasin, 15 mM DTT, 10 mM dNTP, 100 ng Random Primers (Promega), 400 ng Anchored Oligo $(dT)_{20}$ Primer (Invitrogen), 100 U Superscript III Reverse Transcriptase (Life Tech), and DEPC-treated water according to manufactures protocol and stored at −20°C. Clone Manager software (Sci Ed Software) was used to design primers that cross at least one intron-exon boundary. In order to confirm that STIM1 was knocked out, STIM1 primers were designed to include part of exon 2 (see Table 1). Single-cell PCR conditions were optimized for primer concentration, magnesium concentration and annealing temperature. Standard curves were generated using hypothalamic cDNA with dilutions from 1:50 to 1:12,800 for primers used for quantitative PCR (qPCR) to determine the efficiency ($E = 10^{(-1/m)} - 1$; Table 1). Primer pairs with efficiencies of 90–100% permit the use of the comparative ΔΔCT method for analysis (Livak and Schmittgen, 2001; Pfaffl, 2001).

PCR for *Kiss1*, *Stim1*, *Trpc4*, and *Trpc5* mRNAs was performed on 3 µl of cDNA from single cells in a 30-µl reaction volume containing 1× GoTaq Flexi buffer (Promega), 2 mM $MgCl_2$, 10 mM dNTP, 0.33 µM forward and reverse primers, 2 U GoTaq Flexi Polymerase (Promega), and 0.22 µg TaqStart Antibody (Clontech). A total of 45–50 cycles of amplification were performed on a Bio-Rad C1000 thermocycler and the resulting product visualized with ethidium bromide on a 2% agarose gel.

qPCR was performed on 4 µl of cDNA from pools of 10 cells (three to four pools per animal) in duplicate for the target genes (*Stim1*, *Stim2*, *Trpc4*, and *Trpc5*) and 2 µl in duplicate for the reference gene (*Gapdh*) in a 20 µl reaction volume containing 1× Power SYBR Green PCR Master Mix (Applied Biosystems) and 0.5 µM forward and reverse primers. Forty cycles of amplification were run on a Quant Studio 7 Flex Real-Time PCR System (Applied Biosystems) and the resulting data were analyzed using the comparative ΔΔCT method (Livak and Schmittgen, 2001; Pfaffl, 2001). The relative linear quantity was determined with the $2^{-\Delta\Delta CT}$ equation (Bosch et al., 2013). The mean of all of the ΔCT values (ΔCT = CT of the target gene – CT of the reference gene) from the controls was used as the calibrator and the data are expressed as fold change in gene expression.

Drugs

A standard artificial cerebrospinal fluid was used (Qiu et al., 2011). All drugs were purchased from Tocris Bioscience unless otherwise specified. TTX was purchased from Alomone Labs (1 mM), DL-amino-5-phosphonovaleric acid (AP5; 50 mM) and 6-cyano-7-nitroquinoxaline-2,3-dione (CNQX; 10 mM) were dissolved in H_2O. Thapsigargin (Tg; 2 mM), Picrotoxin (100 mM), TacR3 agonist senktide (1 mM), and TRPC4/5 antagonist, HC070 (from MedChemExpress, 10 mM), and 2-aminoethyl diphenylborinate (2-APB, 100 mM) were prepared in dimethylsulfoxide (DMSO). 1,2-Bis(2-aminophenoxy)ethane-N,N,N′,N′-tetraacetic acid (BAPTA) tetrasodium salt (10 mM) replaced EGTA in the internal solution. Aliquots of the stock solutions were stored as appropriate until needed.

Data analysis

For qPCR four Kiss1 neuronal pools (10 cells/pool) from each animal were run in duplicate for the mRNAs that encode for STIM1, STIM2 and GAPDH and the mean value of each gene from each animal ($n = 3$ animals) was used for statistical analysis. Data are expressed as mean ± SEM and were analyzed using an unpaired Student's *t* test. In addition, Kiss1 neuronal pools (10 cells/pool) were used to determine the expression of *Trpc4* and *Trpc5* in these neurons. For scRT-PCR the number of Kiss1-positive cells harvested from *Kiss1*$^{Cre:GFP}$ females injected with Cre-dependent ChR2-mCherry or from *Kiss1*$^{Cre:GFP}$*::Ai32* females were used to qualitatively assess the number of Kiss1 neurons with *Stim1*, *Stim2*, *Trpc4*, *Trpc5*, and percent expression.

Comparisons between different treatments were performed using a repeated measures, two-way or one-way ANOVA analysis with the *post hoc* Bonferroni's test. Differences were considered statistically significant if $p < 0.05$. All data are expressed as mean ± SEM.

Results

Validation of conditional deletion of *Stim1* in Kiss1 neurons

STIM1 is involved in the regulation of neuronal firing in cerebellar Purkinje neurons (Hartmann et al., 2014; Ryu et al., 2017),

midbrain dopaminergic neurons (Sun et al., 2017) and hypothalamic arcuate nucleus POMC neurons (Qiu et al., 2018b). Initially to determine whether STIM1 regulates Kiss1^{ARH} neuronal excitability, we measured the mRNA expression of *Stim1* and its close homolog *Stim2* in manually harvested Kiss1^{ARH} neurons by quantitative real-time PCR (Fig. 1*A*). Based on the qPCR, mRNA levels of *Stim1* were greater than those of *Stim2* in Kiss1^{ARH} neurons (Fig. 1*A1*). Likewise, in cerebellar Purkinje neurons, *Stim1* is also much more abundant than *Stim2* (Hartmann et al., 2014), while in hippocampal (Berna-Erro et al., 2009) and cortical neurons (Gruszczynska-Biegala et al., 2011) *Stim2* expression levels exceed those of *Stim1*. A qualitative, unbiased sampling of Kiss1^{ARH} neurons ($n = 60$) from ovariectomized *Kiss1^{Cre}* females ($n = 3$) revealed that *Stim1* mRNA was expressed in 81.7 ± 7.6% and *Stim2* mRNA was detected in 81.2 ± 2.7% of Kiss1^{ARH} neurons with 70% of neurons expressing both *Stim1* and *Stim2*.

To elucidate the functional role of STIM1 in Kiss1 neurons, we generated mice that lacked STIM1 selectively in Kiss1 neurons (*Stim1^{kko}*; detailed in Materials and Methods). We confirmed the *Stim1* deletion in *Stim1^{kko}* mice using single-cell qPCR of pools of harvested Kiss1^{ARH} neurons ($n = 3$ animals; Fig. 1*A2*). Consistent with the scRT-PCR results (Fig. 1*B*), *Stim1* mRNA was undetectable in *Stim1^{kko}* neurons (Fig. 1*A2*), whereas there was no reduction in *Stim2* mRNA expression (Fig. 1*A3*). In contrast, *Stim1* mRNA was still expressed in the majority of adjacent nonfluorescent neurons obtained from both *Stim1^{kko}* and *Kiss1^{Cre}* mice.

Stim1 deletion reduces SOCE

SOCE constitutes an important source of calcium entry and signaling in neurons. Depletion of ER Ca^{2+} stores causes the ER Ca^{2+} sensor STIM proteins (STIM1 and STIM2) to interact with and activate cell surface Ca^{2+} release-activated Ca^{2+} (CRAC) channels, thereby resulting in a second wave of cytoplasmic Ca^{2+} rise (Moccia et al., 2015). Genetic suppression of *Stim1* in neural progenitor cells results in abrogation of this second wave of calcium rise that constitutes SOCE (Somasundaram et al., 2014). We asked whether deletion of *Stim1* in Kiss1^{ARH} neurons (*Stim1^{kko}*)

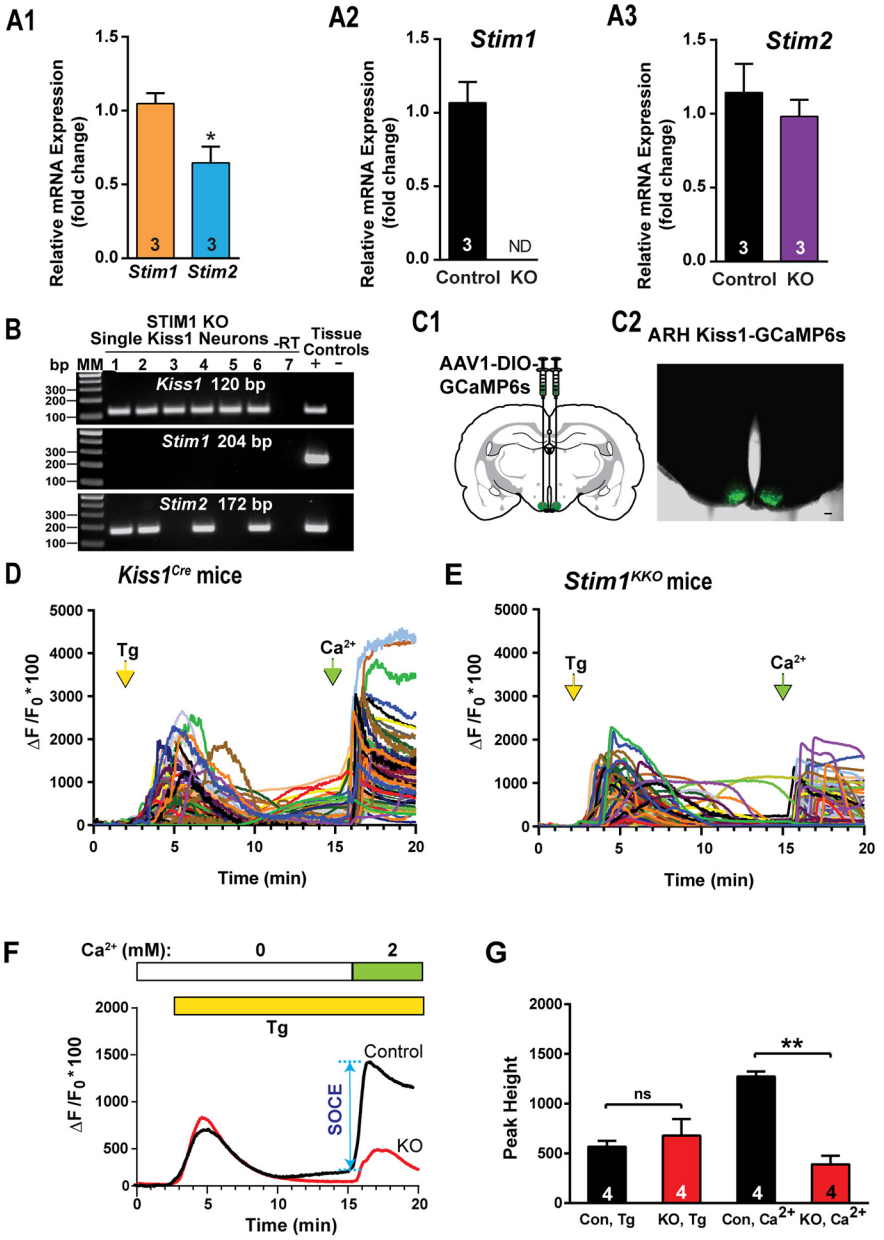

Figure 1. Expression patterns of *Stim1* and *Stim2* in the arcuate Kiss1 neurons. ***A1–A3***, qPCR assay measuring *Stim1* and *Stim2* mRNA in Kiss1^{ARH} neuronal pools ($n = 3$ animals, 10 cells in each pool, 4 pools/animal) from *Kiss1^{Cre}* control and *Stim1^{kko}* female mice ($n = 3$ animals per group). ***A1***, Comparison between *Stim1* and *Stim2* in controls only. Bar graphs represent mean ± SEM (unpaired *t* test, $t_{(4)} = 3.079$, $^{*}p = 0.0370$). ***A2***, *Stim1* was non-detectable (ND) in the STIM1^{KKO} neuronal pools (unpaired *t* test, $t_{(4)} = 7.559$, $^{**}p = 0.0016$). ***A3***, The *Stim2* expression level of Kiss1^{ARH} neurons was not different between *Kiss1^{Cre}* control and *Stim1^{kko}* female mice (unpaired *t* test, $t_{(4)} = 0.7143$, $p = 0.5145$). ***B***, Representative gels illustrating mRNA expression of *Stim1* and *Stim2* in single Kiss1^{ARH} neurons from *Stim1^{kko}* mice. The expected base pair (bp) sizes are *Kiss1*, 120 bp; *Stim1*, 204 bp; *Stim2*, 172 bp. A single neuron was processed without reverse transcriptase (–RT) and RNA extracted from hypothalamic tissue was used as positive (+, with RT) and negative (–, without RT) tissue controls. MM, molecular marker. ***C***, left, Schematic of a coronal section showing the bilateral viral injections in the ARH with AAV-DIO-GCaMP6s. Right, Photomicrograph showing a coronal section confirming targeted bilateral injections of DIO-GCaMP6s into the ARH. ***D***, ***E***, Representative traces of GCaMP6s activity based on cytosolic Ca^{2+} measurements in Kiss1^{ARH} neurons from *Kiss1^{Cre}:GCaMP6s* mice (***D***) and *Stim1^{kko}:GCaMP6s* mice (***E***). ER Ca^{2+} stores were depleted with 2 μM Tg, a SERCA inhibitor, after 20 min of perfusion with aCSF containing 0 mM Ca^{2+}. SOCE was evaluated by substituting the extracellular aCSF containing 0 mM Ca^{2+} with aCSF containing 2 mM Ca^{2+}. ***F***, Averaged traces from ***D***, ***E*** revealed that deletion of *Stim1* in Kiss1^{ARH} neurons attenuated the SOCE. ***G***, Bar graphs summarizing the effects of depletion of Ca^{2+} store by Tg and Ca^{2+} influx (SOCE) in Kiss1^{ARH} neurons from *Kiss1^{Cre}:GCaMP6s* and *Stim1^{kko}:GCaMP6s* mice (two-way ANOVA: main effect of treatment ($F_{(1,3)} = 13.84$, $p = 0.0338$), main effect of time ($F_{(1,3)} = 5.199$, $p = 0.1069$), and interaction ($F_{(1,3)} = 52.14$, $p = 0.0055$); n = number of slices; *post hoc* Bonferroni test, $^{**}p < 0.01$, for SOCE; ns = not significant for depletion of Ca^{2+} store.

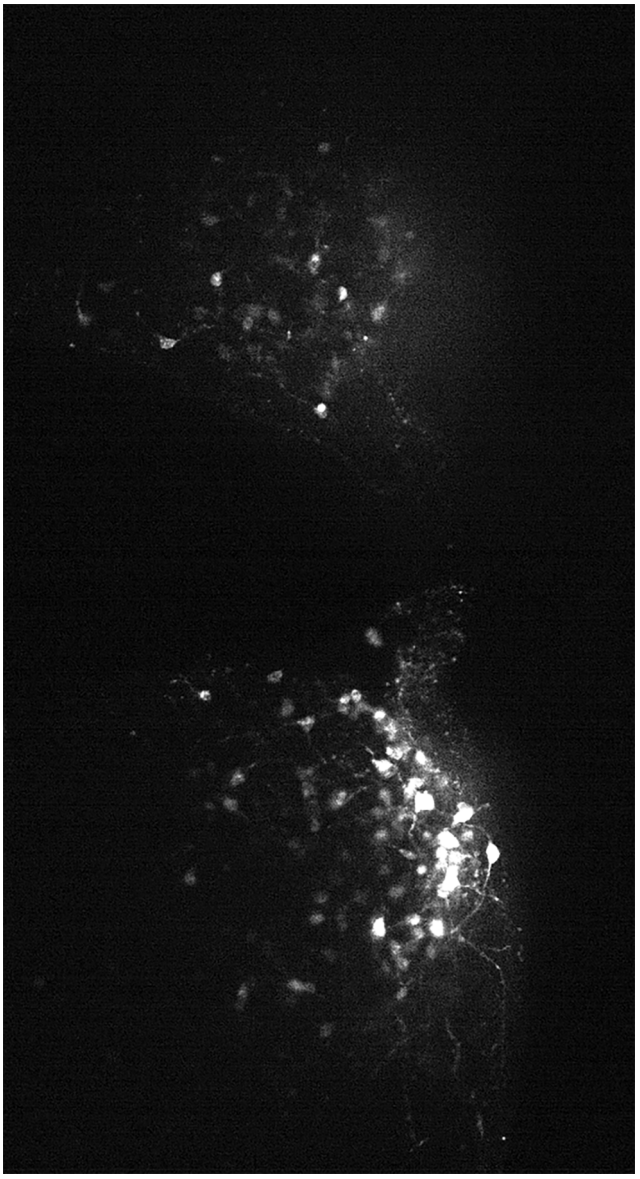

Movie 1. NKB receptor agonist senktide induces $[Ca^{2+}]_i$ increase in Kiss1^{ARH} neurons expressing GCaMP6s. Imaging of transient Ca^{2+} changes in an arcuate slice using spinning disk confocal microscopy. Fluorescence intensity was measured over 20 min, before and after application of senktide (1 μM). The period represented is 20 min. [View online]

attenuates neuronal SOCE. *Kiss1*^{Cre} and *Stim1*^{kko} mice received bilateral ARH injections of GCaMP6 viral vector (Fig. 1*C1*,*C2*), and Kiss1^{ARH} neurons expressing GCaMP6s were imaged using spinning disk confocal microscopy (Movie 1). ER Ca^{2+} stores were released by treatment with 2 μM Tg, a blocker of the sarcoplasmic/endoplasmic reticulum Ca^{2+} ATPase (SERCA) pump. As expected, Tg treatment of neurons bathed in Ca^{2+}-free aCSF generated an initial wave of cytoplasmic Ca^{2+} release ($[Ca^{2+}]_i$) as measured by an increase in GCaMP6s activity both in control and *Stim1*-deleted neurons (Fig. 1*D–F*). As long as neurons were kept in Ca^{2+}-free aCSF, the ER stores remained empty, a situation that was presumably sensed by the Ca^{2+} sensor STIMs. Upon switching to a normal aCSF containing 2 mM Ca^{2+}, an immediate SOCE response was observed as a second wave of cytoplasmic Ca^{2+} rise. Consistent with a role for STIM1 regulation, we observed an attenuation of SOCE in Kiss1^{ARH} neurons from *Stim1*^{kko} mice ($\Delta F/F_0 \times 100 = 1274.5 \pm 49.4$, $n = 4$, *Kiss1*^{Cre} mice vs 389.0 ± 86.1, $n = 4$, *Stim1*^{kko} mice, which was measured from the 15 min time point to the peak; Fig. 1*D–G*), indicating that STIM1 plays a major role in SOCE after Tg-induced ER Ca^{2+} depletion in Kiss1^{ARH} neurons as has been shown in other CNS neurons (Guner et al., 2017; Pavez et al., 2019).

TacR3-induced increase in $[Ca^{2+}]_i$ is augmented by deletion of *Stim1*

TacR3 classically couples to a Gαq protein-calcium signaling and excites Kiss1^{ARH} neurons (de Croft et al., 2013; Ruka et al., 2013; Qiu et al., 2016). Calcium is of critical importance to neurons as it participates in the transmission of depolarizing signals and contributes to synaptic activity (Brini et al., 2014). Therefore, we tested whether STIM1 can modulate TacR3-mediated calcium responses. We first measured the effects of the TacR3, which is Gq-coupled, agonist senktide on GCaMP6s-expressing Kiss1^{ARH} neurons in arcuate slices from *Kiss1*^{Cre} mice; senktide (1 μM) rapidly induced an increase in $[Ca^{2+}]_i$ (Fig. 2*A*,*C*). Next, we investigated whether STIM1 contributes to intracellular rise in $[Ca^{2+}]_i$ after senktide activation. Indeed, deletion of *Stim1* significantly augmented the peak TacR3-mediated response by ~3-fold [$\Delta F/F_0 \times 100 = 244.0 \pm 27.7$, $n = 7$ slices, *Kiss1*^{Cre} mice vs 622.1 ± 133.2, $n = 6$ slices, *Stim1*^{kko} mice; two-way ANOVA: main effect of treatment ($F_{(1,11)} = 5.265$, $p = 0.0424$), main effect of time ($F_{(19,209)} = 42.69$, $p < 0.0001$), and interaction ($F_{(19,209)} = 6.486$, $p < 0.0001$); *post hoc* Bonferroni test, $^{****}p < 0.001$, $^{**}p < 0.01$, $^{*}p < 0.05$; Fig. 2*B*,*C*]. Likewise, the AUC was significantly increased in the *Stim1*^{kko} group by 4-fold (*Kiss1*^{Cre}: 954.8 ± 200.4, $n = 7$ vs *Stim1*^{kko}: 3746.0 ± 1227.0, $n = 6$; Fig. 2*D*).

Deletion of *STIM1* enhances slow EPSP in Kiss1^{ARH} neurons

Kiss1^{ARH} neurons are the chief component of the GnRH pulse generator circuit (Navarro et al., 2009, 2011; Lehman et al., 2010; Okamura et al., 2013), such that they synchronize their activity to trigger the release of peptides to drive pulsatile release of GnRH (Qiu et al., 2016; Clarkson et al., 2017). To investigate whether STIM1 modulates the activity of Kiss1^{ARH} neurons, we bilaterally injected AAV1-Ef1a-DIO-ChR2:mCherry into the arcuate nucleus of *Kiss1*^{Cre} and *Stim1*^{kko} mice. To verify that *Trpc5* mRNAs is co-localized in these Kiss1^{ARH} neurons, we harvested 50 Kiss1^{ARH} neurons from two females and did scRT-PCR for *Trpc5* and *Trpc4* expression. The single-cell analysis revealed that *Trpc5* transcript was detectable in 82% of Kiss1^{ARH} neurons, but *Trpc4* mRNA was not detected in Kiss1^{ARH} neurons (Fig. 3*A*). Moreover, quantitative single-cell PCR documented that *Trpc5* but not *Trpc4* mRNA was expressed in Kiss1^{ARH} neurons (Fig. 3*B*). Initially, whole-cell patch recording in Kiss1^{ARH} neurons from ovariectomized *Kiss1*^{Cre} or *Stim1*^{kko} female mice revealed that there was no difference in the resting membrane potential (RMP: *Kiss1*^{Cre}: -66.0 ± 1.7 mV, $n = 38$ vs *Stim1*^{kko}: -68.2 ± 0.9 mV, $n = 58$) or membrane capacitance (C_m: *Kiss1*^{Cre}: 25.0 ± 1.0 pF, $n = 38$ vs *Stim1*^{kko}: 27.3 ± 0.9 pF, $n = 58$). However, there was a significant difference in the membrane input resistance (R_{in}: *Kiss1*^{Cre}: $524.2 \pm 42.4\,\Omega$, $n = 38$, vs *Stim1*^{kko}: $417.3 \pm 26.9\,\Omega$, $n = 58$, unpaired two-tailed t test, $t_{(94)} = 2.242$, $p = 0.0273$; Table 2), which has also been reported with *Stim1* knockout in cerebellar Purkinje neurons (Ryu et al., 2017). We also measured the rheobase in the presence of synaptic blockers (CNQX, AP5, and picrotoxin) and the frequency-current relationship, and there were no differences between control *Kiss1*^{Cre} and *Stim1*^{kko} mice (Fig. 3*C*,*D*).

Kiss1^{ARH} neurons expressing ChR2-mCherry in slices were photostimulated at 20 Hz for 10 s (Movie 2) to generate slow

EPSPs as previously described (Qiu et al., 2016). As we had hypothesized, deletion of *Stim1* increased the amplitude and the duration of the slow EPSP induced by high-frequency optogenetic stimulation (Fig. 3*E–H*). Therefore, these results indicate that STIM1 expression governs the activity of TRPC5 channels, which ultimately contributes to the synchronous activity of Kiss1^{ARH} neurons.

NKB agonist activates TRPC5 channels in Kiss1^{ARH} neurons from *Kiss1^{Cre}* and *Stim1^{kko}* mice

Based on our previous findings that TPRC5 channel protein is expressed in Kiss1^{ARH} neurons and is activated by the NKB agonist senktide (Qiu et al., 2011; Kelly et al., 2018), we investigated the contribution of TRPC5 channels to generating the inward current underlying the slow EPSP. In the presence of TTX to block voltage-gated Na^+ channels, we observed that senktide induced larger inward currents in Kiss1^{ARH} neurons from *Stim1^{kko}* mice versus *Kiss1^{Cre}* mice (Fig. 4*A*,*D*,*F*,*G*). The senktide-induced cation current was increased by ~2-fold as a result of *Stim1* deletion (*Stim1^{kko}*: 96.4 ± 9.2 pA, $n = 6$, vs *Kiss1^{Cre}*: 56.4 ± 9.8 pA, $n = 7$, unpaired t test, $t_{(11)} = 2.929$, $p = 0.0137$). We also antagonized the effects of senktide with the TPRC1,3,4,5,6 channel blocker 2-APB (Clapham et al., 2005) or with the more selective TRPC4,5 channel blocker HC070 (Just et al., 2018). HC070 suppressed the senktide-induced inward current in Kiss1^{ARH} neurons by 45% in *Kiss1^{Cre}* mice and 42% in *Stim1^{kko}* mice, respectively (Fig. 4*B*,*E–G*), whereas 2APB was more efficacious to inhibit (65%) the senktide-induced inward current in Kiss1^{ARH} neurons (Fig. 4*C*,*F*). Since *Trpc4* mRNA is not expressed in Kiss1^{ARH} neurons (Fig. 3), we would argue that TRPC5 channels mediate the slow EPSP in these neurons. The I–V plots recorded using an Cs^+ internal solution revealed that the slope conductance induced by senktide between −40 to −20 mV was increased (Fig. 4*H*,*I*) by 2.5-fold (*Kiss1^{Cre}*: 0.7 ± 0.2 nS, $n = 16$, vs *Stim1^{kko}*: 1.8 ± 0.5 nS, $n = 10$, unpaired two-tailed t test, $t_{(24)} = 2.172$, $p = 0.0399$), but the reversal potential for the current was not different between Kiss1^{ARH} neurons recorded from *Stim1^{kko}* mice or *Kiss1^{Cre}* mice (*Kiss1^{Cre}*: −13.9 ± 1.6 mV, $n = 16$, vs *Stim1^{kko}*: −14.7 ± 2.1 mV, $n = 10$, unpaired two-tailed t test, $t_{(24)} = 0.3200$, $p = 0.7518$; Fig. 4*J*), indicating that another conductance was not contributing to the increased current.

Chelating $[Ca^{2+}]_i$ with BAPTA abolishes the slow EPSP and persistent firing

Similar to a number of cortical neurons (Zylberberg and Strowbridge, 2017), Kiss1^{ARH} neurons appear to express the biophysical properties that allow them to continue to persistently fire even after a triggering synaptic event has subsided. The "intrinsic bi-stability" of a neuron that generates the persistent firing activity has been linked to a calcium-activated, non-specific cation current (I_{CAN}; Zylberberg and Strowbridge, 2017). TRPC channels, specifically TRPC5 channels, are thought to be responsible for the I_{CAN} current in cortical neurons (Zhang et al., 2011). Therefore, we hypothesized that with TacR3 activation there is an influx of Ca^{2+} through TRPC5 channels leading to greater build-up of $[Ca^{2+}]_i$ (Fig. 2) that facilitates the opening of more TRPC5 channels in a self-sustaining manner, and buffering with 10 mM BAPTA should attenuate the response (Blair et al., 2009). We used our standard optogenetic protocol to activate the slow EPSP and persistent firing of Kiss1^{ARH} neurons. Notably, 10 mM BAPTA inhibited the slow EPSP by ~80% in both control (13.3 ± 1.7 vs 3.1 ± 0.5 mV) and *Stim1^{kko}* (21.0 ± 2.2 vs 5.6 ± 2.4 mV), ovariectomized females (Fig. 5*A–F*). This would indicate that I_{can} through TRPC5 channels generates a slow EPSP that causes the persistent firing in Kiss1^{ARH} neurons.

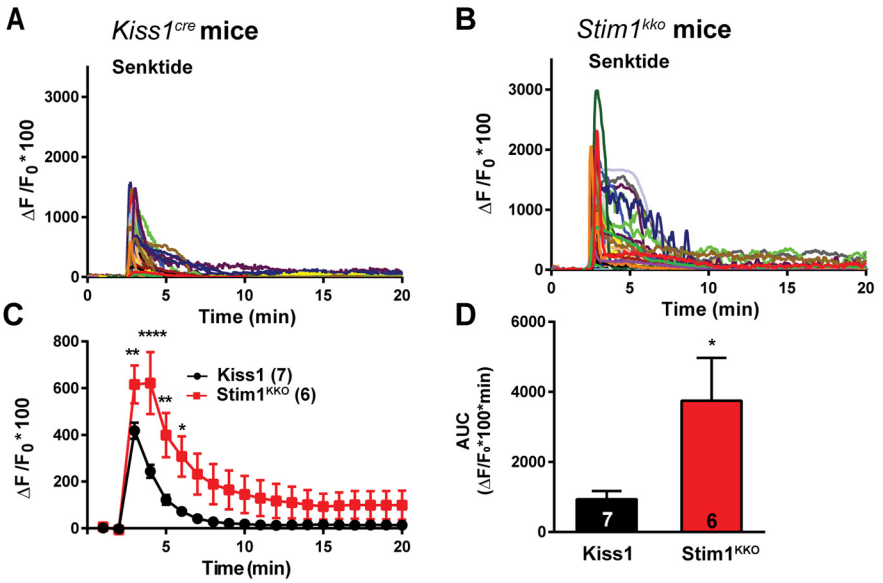

Figure 2. Senktide-induced increase in $[Ca^{2+}]_i$ is augmented by deletion of *Stim1* in GCaMP6s-expressing Kiss1^{ARH} neurons from *Stim1^{kko}* mice. ***A***, ***B***, Representative traces of senktide-induced $[Ca^{2+}]_i$ in Kiss1^{ARH} neurons from *Kiss1^{Cre}* (***A***) and *Stim1^{kko}* (***B***) mice. Traces represent individual cells within a single slice. ***C***, Summary of the potentiation of senktide-induced $[Ca^{2+}]_i$ by deletion of *Stim1*. Two-way ANOVA: main effect of treatment ($F_{(1,11)} = 5.265$, $p = 0.0424$), main effect of time ($F_{(19,209)} = 42.69$, $p < 0.0001$), and interaction ($F_{(19,209)} = 6.486$, $p < 0.0001$); n = number of slices; *post hoc* Bonferroni test, ****$p < 0.001$, **$p < 0.01$, *$p < 0.05$. ***D***, AUC of Kiss1^{ARH} neurons from *Kiss1^{Cre}* and *Stim1^{kko}* mice from ***C***. There was a significant difference (unpaired t test, $t_{(11)} = 2.430$, *$p = 0.0334$) between the two groups.

Stim1 deletion in Kiss1^{ARH} neurons has minimal effects on estrous cycle

Stim1^{kko} mice on the C57BL/6 background were viable at the expected Mendelian ratio and did not show any difference in the time to vaginal opening (*Stim1^{kko}* mice: postnatal day 30.2 ± 0.8, $n = 21$ vs *Kiss1^{Cre}* mice: postnatal day 29.1 ± 0.8, $n = 19$, unpaired t test, $t_{(38)} = 1.003$, $p = 0.3222$). However, since kisspeptin neurons are responsible for the maintenance of the reproductive cycle (Seminara et al., 2003; d'Anglemont de Tassigny et al., 2007; Mayer et al., 2010), and *Stim1* deletion facilitated the synchronous firing of Kiss1^{ARH} neurons, we measured the effects of *Stim1* deletion in Kiss1 neurons on the estrous cycle. We monitored the estrous cycle of *Stim1^{kko}* and *Kiss1^{Cre}* female mice with vaginal lavage for two weeks before ovariectomy for the metabolic studies (see below). *Stim1^{kko}* female mice exhibited prolonged estrous cycles versus the *Kiss1^{Cre}* females (Fig. 6*A–C* vs *D–F*) with a slight decrease in diestrous days and a prolongation of estrous days (Fig. 6*G*,*H*). Although more in depth analysis is warranted (i.e., measurement of pulsatile LH), the results were not unexpected since augmented synchronous activity of Kiss1^{ARH} neurons, as we documented at the cellular level, should

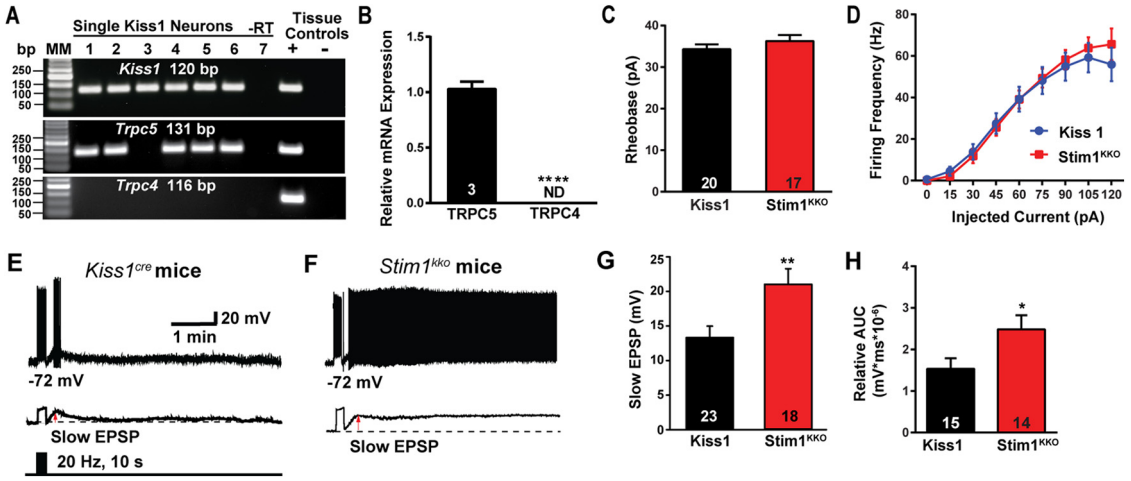

Figure 3. Deletion of *Stim1* augments high-frequency optogenetic stimulation-induced slow EPSP depolarization in Kiss1^{ARH} neurons. ***A***, Representative gel image illustrating the mRNA expression of *Trpc5* channel subunit in Kiss1^{ARH} neurons harvested from female mice. The expected size of PCR products for *Kiss1* and *Trpc5* are indicated. *Trpc4* mRNA was not detected in Kiss1^{ARH} neurons. MM, molecular marker; –RT indicates a harvested Kiss1 neuron reacted without RT; + indicates positive tissue control (with RT); – indicates negative tissue control (without RT) using cDNA from mouse medial basal hypothalamic tissue; RT, reverse transcriptase. ***B***, Quantitative single-cell PCR (3 × 10 cell pools per animal, $n = 3$ animals) verified that *Trpc5* was expressed in Kiss1^{ARH} neurons, whereas *Trpc4* mRNA was not detected (unpaired *t* test, $t_{(4)} = 15.67$, ****$p < 0.0001$). ***C***, The mean rheobase of Kiss1^{ARH} neurons between *Kiss1* and *Stim1^{kko}* groups was not different (unpaired *t* test, $t_{(35)} = 1.042$, $p = 0.3045$). ***D***, There was no difference in the evoked firing rate between *Kiss1* and *Stim1^{KKO}* groups (two-way ANOVA: main effect of treatment, $F_{(1,32)} = 0.08594$, $p = 0.7713$, main effect of time, $F_{(8,256)} = 125.6$, $p < 0.0001$, and interaction, $F_{(8,256)} = 1.359$, $p = 0.2149$; *Kiss1^{Cre}*, n =19, *Stim1^{kko}*, $n = 15$; *post hoc* Bonferroni test, $p > 0.05$). ***E***, ***F***, High-frequency optogenetic stimulation (20 Hz, 10 s) generated slow EPSPs in a ChR2-expressing Kiss1^{ARH} neuron from control *Kiss1^{Cre}* mice (***E***) and in a ChR2-expressing Kiss1^{ARH} neuron from *Stim1^{kko}* mice (***F***). The lower traces show the slow EPSP after low-pass filtering the traces from ***E***, ***F*** (red arrow). ***G***, Summary of the effects of *Stim1* deletion on the slow EPSP amplitude (unpaired *t* test, $t_{(39)} = 2.802$, **$p = 0.0079$). ***H***, Summary of the effects of *Stim1* deletion on the AUC of slow EPSP (unpaired *t* test, $t_{(27)} = 2.246$, *$p = 0.0331$). Bar graphs represent the mean ± SEM. Cell numbers are indicated.

Table 2. Electrophysiological properties of Kiss1^{ARH} neurons from *Kiss1^{cre}* and *Stim1^{kko}* female mice

	RMP (mV)[a]	Rin (MΩ)[b]	Cm (pF)[c]	Rheobase (pA)[d]	Threshold (mV)[e]	Overshoot (mV)[f]	Peak amplitude (mV)[g]	FWHM (ms)[h]	AHP amplitude (mV)[i]
Kiss1^{cre}	−66.0 ± 1.7	524.2 ± 42.4	25.0 ± 1.0	34.3 ± 1.1	−46.1 ± 1.0	55.8 ± 1.9	91.8 ± 2.0	0.9 ± 0.0	30.5 ± 1.7
	$n = 38$	$n = 38$	$n = 38$	$n = 15$	$n = 15$	$n = 15$	$n = 15$	$n = 15$	$n = 15$
Stim1^{KKO}	−68.2 ± 0.9	417.3 ± 26.9*	27.3 ± 0.9	36.2 ± 1.5	−45.4 ± 0.9	56.0 ± 2.7	91.4 ± 2.9	0.9 ± 0.0	32.8 ± 1.7
	$n = 58$	$n = 58$	$n = 58$	$n = 22$	$n = 22$	$n = 22$	$n = 22$	$n = 22$	$n = 22$

RMP, resting membrane potential; Rin, input resistance; Cm, membrane capacitance; FWHM, full-width at half-maximum of the AP; AHP, afterhyperpolarization; *n* = neurons.
[a]$p = 0.2232$
[b]$p = 0.0273$, unpaired two-tailed *t* test, $t_{(94)} = 2.242$
[c]$p = 0.0997$
[d]$p = 0.3045$
[e]$p = 0.6296$
[f]$p = 0.9507$
[g]$p = 0.9116$
[h]$p = 0.4476$; [i]$p. = 0.3348$.

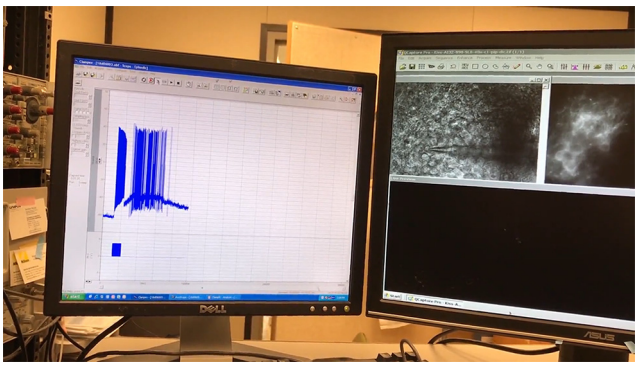

Movie 2. High-frequency photostimulation induces a slow EPSP. Slow EPSP was induced by a 10-s 20-Hz photostimulation (light intensity 0.9 mW and pulse duration, 10 ms) in a ChR2-expressing Kiss1^{ARH} neuron in a slice from a *Kiss1^{Cre}::Ai32* mouse. The period represented is 1 min, 34 s. [View online]

still drive LH pulses in these female mice (Qiu et al., 2016; Clarkson et al., 2017).

Stim1 deletion in Kiss1^{ARH} neurons protects ovariectomized females against diet-induced obesity

Subsequently, the same two cohorts of female mice, *Stim1^{kko}* ($n = 10$) and the littermate control *Kiss1^{Cre}* ($n = 10$) mice, were ovariectomized at around three months of age and put on a HFD for eight weeks (see Materials and Methods). Over this time period, there was significantly less gain in body weight in the *Stim1^{kko}* versus the *Kiss1^{Cre}* mice (Fig. 7*A*,*B*). Moreover, the average fat mass of *Stim1^{kko}* mice was significantly lighter than that of *Kiss1^{Cre}* controls by week 6 (*Stim1^{kko}* vs *Kiss1^{Cre}* mice fat mass: 7.6 ± 0.9 g, $n = 10$ vs 11.4 ± 1.1 g, $n = 10$; Fig. 7*C*). The lean mass of *Stim1^{kko}* mice was also significantly less versus the *Kiss1^{Cre}* mice (*Stim1^{kko}* vs the *Kiss1^{Cre}* mice lean mass: 16.9 ± 0.4 g, $n = 10$ vs 18.9 ± 0.4 g, $n = 10$; Fig. 7*D*). After six weeks, both *Stim1^{kko}* and *Kiss1^{Cre}* controls were assessed for glucose tolerance

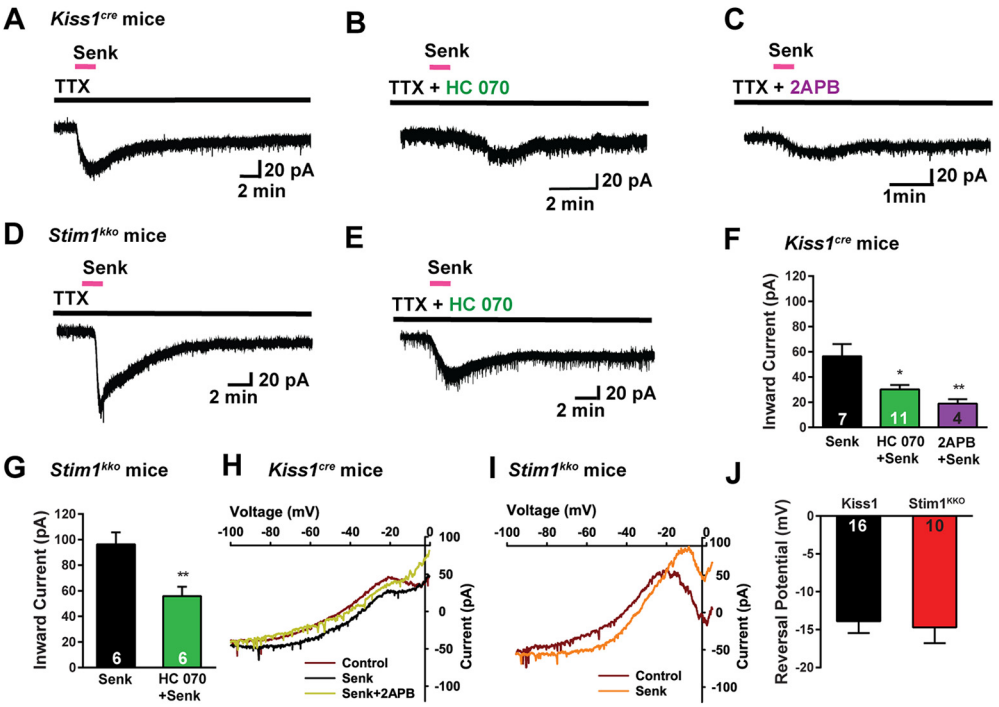

Figure 4. *Stim1* deletion augments senktide-induced Kiss1^{ARH} neuronal excitability through TRPC channel activation. ***A–C***, Representative traces of senktide (1 μM)-induced inward current in the absence (***A***) or presence of TRPC4/5 channel blocker HC070 (***B***, 100 nM) or 2APB (***C***, 100 μM) from *Kiss1*^{Cre} mice in the presence of fast sodium channel blockade (TTX, 1 μM). $V_{hold} = -60$ mV. ***D–E,*** *Stim1* deletion augments senktide-induced inward current (***D***), which is antagonized by the TRPC4/5 channel blocker HC070 (***E***, 100 nM). ***F***, Summary of the effects of HC070 and 2APB on senktide-induced inward current in Kiss1^{ARH} neurons from *Kiss1*^{Cre} mice. Comparisons between different treatments were performed using a one-way ANOVA analysis ($F_{(2,19)} = 7.737$, $p = 0.0035$ with the Newman–Keuls's *post hoc* test; *$p < 0.05$ or **$p < 0.01$ vs control). ***G***, Summary of the effects of HC070 on senktide-induced inward current in Kiss1^{ARH} neurons from *Stim1*^{kko} mice (unpaired *t* test, $t_{(10)} = 3.457$, *$p = 0.0062$). ***H***, ***I***, The I–V relationships before and during the peak response to senktide (Senk) in Kiss1^{ARH} neurons from *Kiss1*^{Cre} (***H***) and *Stim1*^{kko} (***I***) mice indicated that although the slope conductance increased by 2.5-fold, the reversal potential of the nonselective cation current (~−14 mV) did not change. Note, the TRPC channel blocker 2APB clearly abrogated the senktide response (***H***). ***J***, Summary of the reversal potentials of the senktide-induced cation current recorded in Kiss1^{ARH} neurons from *Kiss1*^{Cre} and *Stim1*^{kko} mice. Bar graphs represent the mean ± SEM (unpaired two-tailed *t* test, $t_{(24)} = 0.3200$, $p = 0.7518$). Cell numbers are indicated.

using an intraperitoneal GTT (see Materials and Methods). Both *Stim1*^{kko} and *Kiss1*^{Cre} females started at relatively the same blood glucose levels after an overnight fast (Fig. 7*E*, time 0), suggesting similar whole-body homeostatic conditions after fasting. However, *Stim1*^{kko} female mice had significantly lower glucose levels after intraperitoneal glucose compared with *Kiss1*^{Cre} females, indicating that *Stim1*^{kko} females were more glucose tolerant compared with *Kiss1*^{Cre} controls. *Stim1*^{kko} females had a significantly higher glucose clearance rate than controls based on the integrated AUC (*Stim1*^{kko} vs the *Kiss1*^{Cre} controls AUC: 20,232 ± 868 mg/dl/min, $n = 6$ vs 22,622 ± 624 mg/dl/min, $n = 6$). Finally, when both groups were euthanized after eight weeks on HFD and the tissues harvested, both the intrascapular brown adipose tissue (iBAT) and perigonadal adipose tissue (GAT) were dissected from each mouse and weighed. Both iBAT and GAT masses were significantly lighter in the *Stim1*^{kko} versus the *Kiss1*^{Cre} females (*Stim1*^{kko} vs the *Kiss1*^{Cre} iBAT: 73.3 ± 6.0 mg, $n = 10$ vs 97.3 ± 9.6 mg, $n = 10$; *Stim1*^{kko} vs the *Kiss1*^{Cre} GAT: 1.5 ± 0.2 g, $n = 10$ vs 2.3 ± 0.2 g, $n = 10$; Fig. 7*F*,*G*). Overall, these results suggest that conditional deletion of *Stim1* in Kiss1^{ARH} neurons affords some protection against diet-induced obesity. However, we cannot overlook the possibility that deletion of *Stim1* in Kiss1-expressing hepatocytes might contribute to this metabolic phenotype (Song et al., 2014).

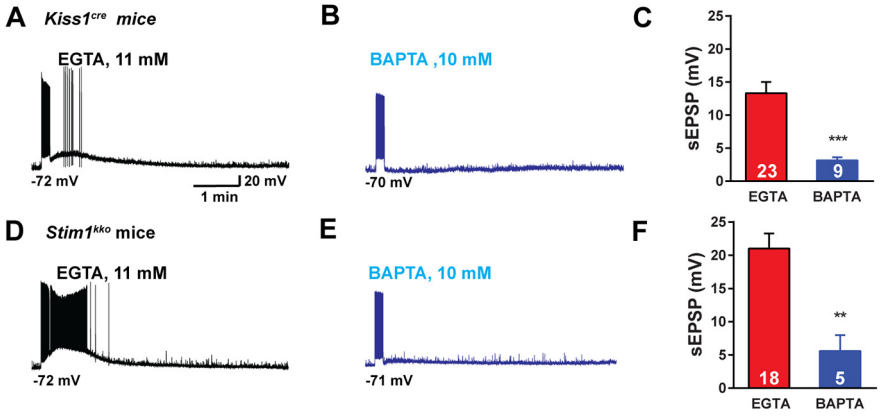

Figure 5. *Stim1* deletion augmentation of senktide-induced Kiss1^{ARH} neuronal excitability is dependent on intracellular calcium. ***A***, ***B***, High-frequency photostimulation-induced slow EPSP recorded using normal internal solution (***A***, EGTA 11 mM) and BAPTA internal solution (***B***, EGTA was replaced by 10 mM BAPTA) in Kiss1^{ARH} neurons from *Kiss1*^{Cre} mice. ***C***, Summary of the effects of buffering intracellular calcium on the slow EPSP in ***A***, ***B*** (unpaired *t* test, $t_{(30)} = 3.741$, ***$p = 0.0008$). ***D***, ***E***, High-frequency photostimulation-induced slow EPSP recorded using normal internal solution (***D***, EGTA 11 mM) and BAPTA internal solution (***E***) in Kiss1^{ARH} neurons from *Stim1*^{KKO} mice. ***F***, Summary of the effects of buffering intracellular calcium on the slow EPSP in ***D***, ***E*** (unpaired *t* test, $t_{(21)} = 3.425$, **$p = 0.0025$). Data points represent the mean ± SEM. Cell numbers are indicated.

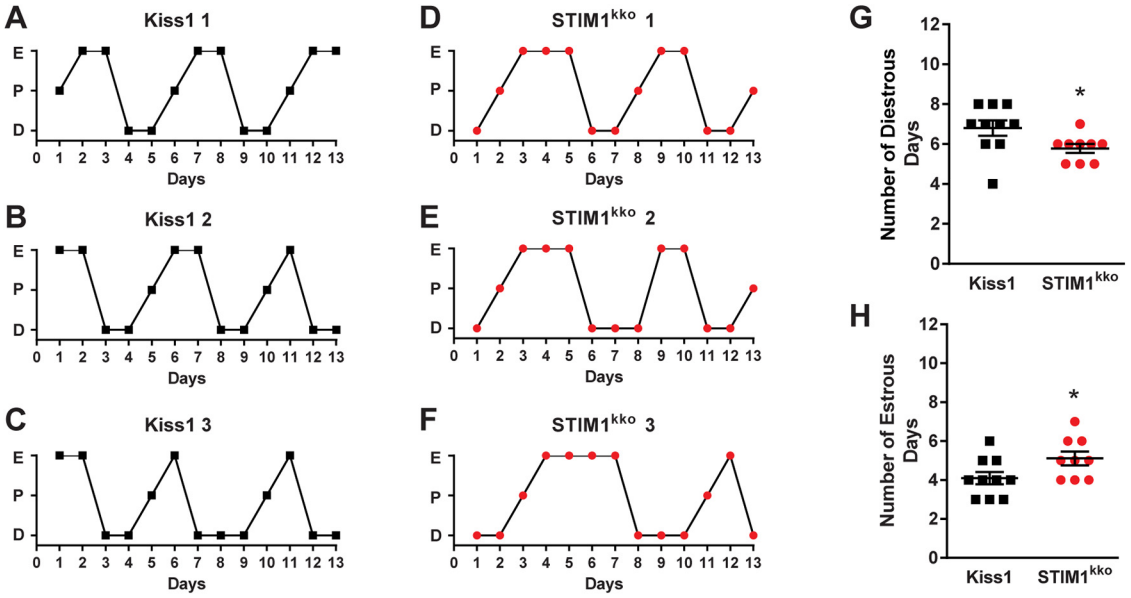

Figure 6. *Stim1*^{kko} mice exhibit more estrous days. ***A–F***, Representative estrous cycle data from three representative control *Kiss1*^{Cre} and three *Stim1* ^{kko} mice over a 13-d period. Vaginal lavage was done daily at 9:30 A.M., and cell cytology was observed and recorded as diestrus (***D***), proestrus (***P***), or estrus (***E***). Summary data for the number of diestrous days (***G***) and estrous days (***H***) during the 13-d period was compared between *Kiss1*^{Cre} ($n = 10$) and *Stim1* ^{kko} mice ($n = 9$; unpaired, two-tailed t test for ***G***, $t_{(17)} = 2.215$, $^*p = 0.0407$; unpaired two-tailed t test for ***H***, $t_{(17)} = 2.151$, $^*p = 0.0461$).

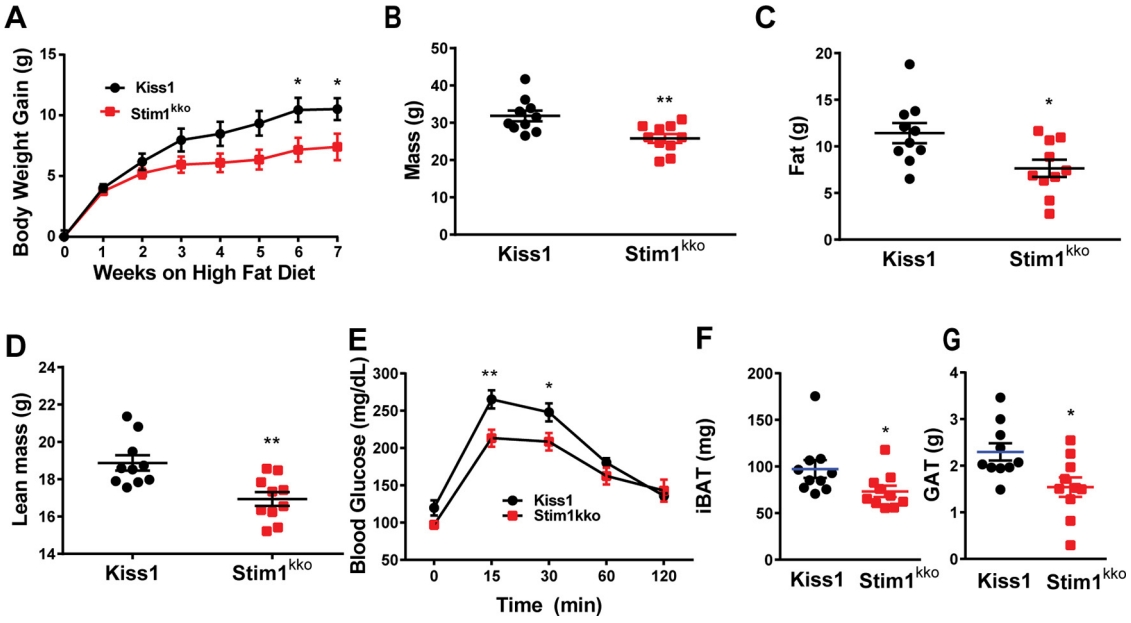

Figure 7. Ablation of *Stim1* in Kiss1 neurons attenuates body mass, fat, and lean in mice on a HFD. *Stim1*^{kko} and *Kiss1*^{Cre} littermate control females were ovariectomized and fed a HFD (45% kcal from fat) for seven weeks. ***A***, Body-weight gain measured once a week for seven weeks. The HFD caused significant weight gain in both groups relative to their baseline with the *Kiss1*^{Cre} females gaining significantly more weight by six weeks [two-way ANOVA: main effect of treatment ($F_{(1,18)} = 3.839$, $p = 0.0657$), main effect of time ($F_{(7,126)} = 98.07$, $p < 0.0001$), and interaction ($F_{(7,126)} = 4.645$, $p = 0.0001$); *Kiss1* control, $n = 10$, *Stim1*^{kko}, $n = 10$; *post hoc* Bonferroni test, $^*p < 0.05$]. ***B–D***, Mass (***B***), total body fat (***C***), and lean mass (***D***) measured by an EchoMRI whole-body composition analyzer. Lean mass did not include bone and fluids within organs. The difference in mass (***B***), body fat (***C***), and lean mass (***D***) between the groups was significantly different by six weeks on HFD (unpaired, two-tailed t test for ***B***, $t_{(18)} = 3.222$, $^{**}p = 0.0047$; unpaired two-tailed t test for ***C***, $t_{(18)} = 2.662$, $^*p = 0.0159$; unpaired, two-tailed t test for ***D***, $t_{(18)} = 3.489$, $^{**}p = 0.0026$). ***E***, Six weeks after HFD, there was a significant difference in GTTs between the two groups [two-way ANOVA: main effect of treatment ($F_{(1,9)} = 6.282$, $p = 0.0335$), main effect of time ($F_{(4,36)} = 88.01$, $p < 0.0001$) and interaction ($F_{(4,36)} = 3.527$, $p = 0.0158$); *Kiss1*^{Cre}, $n = 6$; *Stim1*^{kko}, $n = 5$; *post hoc* Bonferroni test, $^{**}p < 0.01$, $^*p < 0.05$]. ***F***, ***G***, Both iBAT and GAT mass of *Stim1*^{kko} were lighter than that of *Kiss1*^{Cre} mice on a high fat diet after eight weeks (unpaired, two-tailed t test for iBAT, $t_{(18)} = 2.127$, $^*p = 0.0475$; unpaired two-tailed t test for GAT, $t_{(18)} = 2.711$, $^*p = 0.0143$).

Discussion

For the first time, we show that conditional knock-out of *Stim1* significantly reduces SOCE in Kiss1^{ARH} neurons following Tg-mediated depletion of Ca^{2+} stores. Based on single-cell qPCR analysis, *Stim1* mRNA was expressed at approximately 2-fold higher levels than *Stim2* in Kiss1^{ARH} neurons, and deletion of *Stim1* did not alter expression of *Stim2* in Kiss1^{ARH} neurons, i.e., there was no developmental compensation. Selective deletion of

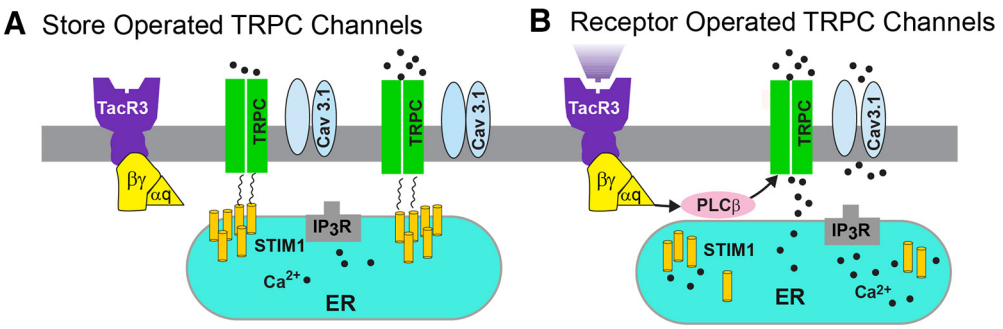

Figure 8. A cellular model of STIM1 affecting NKB activation of TRPC5 channels in Kiss1^{ARH} neurons. SOCE is a conserved mechanism by which the depletion of the ER calcium store is conveyed to calcium-permeable channels at the PM, triggering calcium influx from the extracellular space and into the cell cytosol. A physiological mechanism responsible for the activation of SOCE results from the stimulation of G-protein-coupled receptors associated with the IP_3 and phospholipase C cascade, resulting in the release of calcium from ER, via the IP_3 receptor (IP_3R). ***A***, Under physiological stress and in the absence of E_2, STIM1 interacts with TPRC5 channels thereby engaging these Ca^{2+} channels as store-operated channels, which are activated with ER depletion of Ca^{2+}. ***B***, However, under physiological conditions in reproductively active females, in which E_2 downregulates the expression of *STIM1*, TRPC5 channels are converted to receptor-operated channels in Kiss1^{ARH} neurons. NKB binds to its receptor (TacR3) to activate $G\alpha q$–PLCβ signaling cascade to facilitate TPRC5 channel opening, generating a robust inward Ca^{2+}/Na^{+} current to depolarize Kiss1^{ARH} neurons, activating T-type calcium (Cav3.1) channels to greatly increase Kiss1^{ARH} neuronal excitability.

Stim1 in Kiss1^{ARH} neurons augmented the TacR3-mediated increase in $[Ca^{2+}]_i$ and synchronous activity of Kiss1^{ARH} neurons by almost 4-fold. Whole-cell recording revealed that both the amplitude and the duration of the slow EPSP induced by high-frequency optogenetic stimulation of Kiss1^{ARH}-ChR2 neurons were significantly enhanced by *Stim1* deletion. This augmentation of the slow EPSP was mediated by TacR3 coupling to TRPC5 channel activation since the senktide-induced inward current was equally enhanced. Moreover, the inward current exhibited the signature double rectifying I–V plot of TRPC5 channels and was antagonized by both 2APB and the more selective TRPC 4/5 channel blocker HC070. Furthermore, chelating $[Ca^{2+}]_i$ with BAPTA abolished the slow EPSP and persistent firing of Kiss1^{ARH} neurons. Finally, the enhanced TacR3 signaling in *Stim1*^{kko} female mice translated into more neuroprotection against diet-induced obesity and glucose intolerance.

Mammalian TRPC channels can be activated by G-protein-coupled receptors and receptor tyrosine kinases (Clapham, 2003; Ambudkar and Ong, 2007) and are one of the major targets for Group I metabotropic glutamate receptor (mGluR1) signaling in CNS neurons (Tozzi et al., 2003; Bengtson et al., 2004; Faber et al., 2006; Berg et al., 2007). In substantia nigra dopamine neurons TRPC5 channels are highly expressed, and mGluR1 agonists induce a current that exhibits a double-rectifying I–V plot (Tozzi et al., 2003) similar to the effects of the NKB agonist senktide in Kiss1^{ARH} neurons (Fig. 4). Both mGluR1 and TacR3 are Gq-coupled to phospholipase C (PLC) activation which leads to hydrolyzis of phosphatidylinositol 4,5-biphosphate (PIP_2) to diacylglycerol (DAG) and inositol 1,4,5 triphosphate (IP_3). TRPC channels are cation selective and can associate with Orai calcium channels to form CRAC channels (Birnbaumer, 2009). TRPC5 channels are highly permeable to calcium (P_{Ca}/P_{Na} = 9:1; Venkatachalam and Montell, 2007), and a unique feature of TRPC5 (and TRPC 4) channels is that they are potentiated by micromolar concentrations of lanthanum (La^{3+}; Clapham et al., 2005), which we have exploited to characterize TPRC5 signaling in POMC neurons (Qiu et al., 2010, 2014).

Both leptin and insulin excite/depolarize Kiss1^{ARH} and POMC neurons through activation of TRPC5 channels (Qiu et al., 2010, 2011, 2014; Kelly et al., 2018). More recently, we documented a critical role of STIM1 in the insulin signaling cascade in POMC neurons (Qiu et al., 2018b). *Stim1* mRNA is highly expressed in POMC (Qiu et al., 2018b) and Kiss1^{ARH} neurons (Fig. 1), and E2 downregulates *Stim1* mRNA expression in microdissected arcuate nuclei that encompasses these two populations of neurons. Downregulation of *Stim1* is critical for maintaining insulin excitability in POMC neurons with diet-induced obesity (Qiu et al., 2018b). In ovariectomized females that are relatively refractory to insulin excitation, pharmacological blockade of the SOCE complex quickly increases the insulin-mediated excitation of POMC neurons (i.e., activation of the TRPC5-mediated inward current), which supports the concept that TRPC5 channels play a role both in SOCE and receptor operated calcium entry (Birnbaumer, 2009; Salido et al., 2011). Therefore, selective deletion of *Stim1* in Kiss1 neurons would ensure that TRPC5 channels function as receptor-operated channels to couple TacR3s and transmit the excitatory effects of NKB to induce synchronous firing of Kiss1^{ARH} neurons as demonstrated in the present findings.

Downregulating STIM1 decreases the SERCA-dependent cytosolic Ca^{2+} clearance and elevates intracellular Ca^{2+} levels (Fig. 2; Ryu et al., 2017), which could also contribute to activation of TRPC5 channels in Kiss1^{ARH} neurons (Blair et al., 2009). Indeed, we have found that Ca^{2+} significantly potentiates the leptin-induced TRPC5 current in POMC neurons (Qiu et al., 2010), which has recently been corroborated in primary cultures of POMC neurons (Perissinotti et al., 2021). What is impressive is that *Stim1* deletion not only increased the amplitude, but it also prolonged the duration of the slow EPSP (Fig. 3). The slow EPSP is reminiscent of the "plateau potential" that has been described in hippocampal and cortical neurons (Zhang et al., 2011; Arboit et al., 2020). We know that electrical stimulation (20 Hz) cannot induce the slow EPSP, and the duration is not dependent on the AP firing per se since blockade of sodium channels with QX314, and hence abrogation of AP firing, does little to affect the duration of the depolarization (Qiu et al., 2016). Rather, many neurons express biophysical properties that allow them to continue to persistently fire even after a triggering synaptic event has subsided (Zylberberg and Strowbridge, 2017). Moreover, the intrinsic bi-stability of neurons that generates persistent firing activity has been linked to a calcium-activated, non-specific cation current (Zylberberg and Strowbridge, 2017), and TRPC channels, specifically TRPC5 channels, are thought to be responsible for the I_{CAN} in cortical neurons (Zhang et al., 2011). Therefore, we hypothesized that with TacR3 activation there is an influx of Ca^{+2} through TRPC5 channels leading to greater build-up of $[Ca^{2+}]_i$ (Fig. 2) that facilitates the opening of more TRPC5 channels in a self-sustaining manner. We tested this directly by using

the fast intracellular calcium chelator BAPTA, which has been shown to robustly inhibit TRPC5 channel activation (Blair et al., 2009). Indeed, BAPTA essentially abolished the slow EPSP and persistent firing in Kiss1^{ARH} neurons following optogenetic stimulation in both control and *Stim1*^{kko} female mice (Fig. 5). Moreover, similar to cerebellar Purkinje neurons (Ryu et al., 2017), we measured a significant decrease in the input resistance with *Stim1* deletion, which we believe reflects an increase in distribution of TRPC5 channels across the PM and coupling to Tac3 receptors (Fig. 8; Birnbaumer, 2009). A similar scenario occurs in cortical neurons and in heterologous cells expressing *Cav1.2* (L-type calcium) channels and *Stim1*, where inhibition of STIM1 augments Ca^{2+} influx through L-type calcium channels (Park et al., 2010; Wang et al., 2010). Furthermore, deletion of *Stim1* in cardiomyocyte-derived (HL-1) cells increases the peak amplitude and current density of T-type calcium channels and shifts the activation curve toward more negative membrane potentials (Nguyen et al., 2013). Biotinylation assays have revealed that deletion of *Stim1* increases T-type calcium channel surface expression, and co-immunoprecipitation assays suggest that STIM1 directly regulates T-type channel activity (Nguyen et al., 2013). Thus, STIM1 appears to dampen the activity of voltage-gated calcium channels. Importantly, estradiol treatment downregulates *Stim1* expression in the ARH of ovariectomized female mice and guinea pigs (Qiu et al., 2018b). In contrast, E2 upregulates *Cav3.1* channel expression by 3-fold and whole cell currents by 10-fold in Kiss1^{ARH} neurons, which greatly enhances the excitability and contributes to the synchronous firing of Kiss1^{ARH} neurons (Qiu et al., 2018a). The T-type calcium channel Cav3.1 underlies burst firing in anteroventral periventricular preoptic (AVPV) kisspeptin neurons (Zhang et al., 2013b; Wang et al., 2016) and facilitates TRPC 4 channel activation in GnRH neurons (Zhang et al., 2008, 2013a). Calcium influx via Cav3.1 channels may also facilitate TRPC5 channel opening in Kiss1^{ARH} neurons (Fig. 8), but this remains to be determined.

Presumably with conditional knock-out, *Stim1* was deleted in all cells expressing kisspeptin, which includes arcuate, AVPV and amygdala kisspeptin neurons, and non-neural kisspeptin cells in the gonads, pancreas and liver (Dudek et al., 2019). Currently, we found that the deletion of *Stim1* in kisspeptin neurons had a minor effect on the estrous cycle. *Stim1*^{kko} mice exhibited more estrous-type vaginal cytology, which may be indicative of higher levels of circulating estrogens because of increased synchronous firing of kisspeptin neurons and excitatory drive to GnRH neurons (Qiu et al., 2016; Clarkson et al., 2017). It is important to note that synchronous firing of "pulse-generator" Kiss1^{ARH} neurons is a failsafe system for maintaining gonadotropin pulses and folliculogenesis in female rodents (Nagae et al., 2021).

Because of the well-documented anorexigenic actions of E2 on POMC and Agouti-related peptide (AgRP) neurons controlling energy homeostasis (Qiu et al., 2006; Roepke et al., 2010; Clegg, 2012; Kelly and Rønnekleiv, 2012; Smith et al., 2013), we ovariectomized the females before feeding them a HFD. After seven weeks on a HFD, *Stim1*^{kko} females gained less body weight and showed significantly less body fat and lean mass than ovariectomized *Kiss1*^{Cre} females on a HFD. Most importantly, *Stim1*^{kko} females exhibited improved glucose tolerance. Kiss1^{ARH} neurons probably mediate these protective effects via their input onto POMC and AgRP neurons. Besides the peptides Kiss1^{ARH} neurons also co-express the vesicular glutamate transporter 2 (vGluT2; Cravo et al., 2011; Nestor et al., 2016), and we have documented that optogenetic stimulation of Kiss1^{ARH} neurons expressing ChR2 releases glutamate, which is dependent on the estrogenic state of females (Qiu et al., 2018a). Although the mRNA expression of *Kiss1, Tac2 and Pdyn* mRNA in Kiss1^{ARH} neurons are all downregulated by E2 (Navarro et al., 2009; Lehman et al., 2010), *Vglut2* mRNA expression is upregulated together with increased probability of glutamate release in E2-treated, ovariectomized females (Qiu et al., 2018a). Low-frequency (1–2 Hz) optogenetic stimulation of Kiss1^{ARH} neurons evokes fast ionotropic glutamatergic EPSCs in POMC and AgRP neurons, but high-frequency (20 Hz) optogenetic stimulation releases enough glutamate to induce a slow excitatory response in POMC neurons but a slow inhibitory response in AgRP neurons (Nestor et al., 2016; Qiu et al., 2016, 2018a). Indeed, the Group I mGluR agonist DHPG depolarizes POMC neurons, while Group II/III mGluR agonists (DCG-IV; AMN082) hyperpolarize AgRP neurons (Qiu et al., 2018a). Group I mGluRs (mGluR1 and mGluR5) are G_q/G_{11}-coupled, while Group II/III mGluRs (mGluR2 and mGluR7) are G_i/G_o-coupled (Niswender and Conn, 2010). Hence, the output of Kiss1^{ARH} neurons excites the anorexigenic POMC neurons and inhibits the orexigenic AgRP neurons. Therefore, Kiss1^{ARH} neurons appear to be an integral part of an anorexigenic circuit in the hypothalamus (Qiu et al., 2018a; Rønnekleiv et al., 2019; Navarro, 2020).

Presently, there is compelling evidence that Kiss1^{ARH} neurons are a critical "command" neuron for coordinating energy states with reproductive functions (for review, see Rønnekleiv et al., 2019; Navarro, 2020). We have now documented that conditional knock-out of *Stim1* in Kiss1^{ARH} neurons, which augments the NKB-mediated depolarization of these neurons via TRPC5 channels, helps protect ovariectomized, female mice from diet-induced obesity and glucose intolerance. In addition, in preliminary experiments we have found that insulin treatment *in vitro* increases the synchronous firing (GCaMP6 activity) of Kiss1^{ARH} neurons, which further emphasizes its role as a command neuron. Clearly, Kiss1^{ARH} neurons are part of a hypothalamic circuit for coordinating reproduction with energy balance, but additional experiments are needed to elucidate the cellular mechanisms by which steroid and metabolic hormonal signaling synergize to govern their activity.

References

Ambudkar IS, Ong HL (2007) Organization and function of TRPC channelosomes. Pflugers Arch 455:187–200.

Arboit A, Reboreda A, Yoshida M (2020) Involvement of TRPC4 and 5 channels in persistent firing in hippocampal CA1 pyramidal cells. Cells 9:365.

Asarian L, Geary N (2006) Modulation of appetite by gonadal steroid hormones. Philos Trans R Soc Lond B Biol Sci 361:1251–1263.

Ayala JE, Samuel VT, Morton GJ, Obici S, Croniger CM, Shulman GI, Wasserman DH, McGuinness OP; NIH Mouse Metabolic Phenotyping Center Consortium (2010) Standard operating procedures for describing and performing metabolic tests of glucose homeostasis in mice. Dis Model Mech 3:525–534.

Bengtson CP, Tozzi A, Bernardi G, Mercuri NB (2004) Transient receptor potential-like channels mediate metabotropic glutamate receptor EPSCs in rat dopamine neurones. J Physiol 555:323–330.

Berg AP, Sen N, Bayliss DA (2007) TrpC3/C7 and Slo2.1 are molecular targets for metabotropic glutamate receptor signaling in rat striatal cholinergic interneurons. J Neurosci 27:8845–8856.

Berna-Erro A, Braun A, Kraft R, Kleinschnitz C, Schuhmann MK, Stegner D, Wultsch T, Eilers J, Meuth SG, Stoll G, Nieswandt B (2009) STIM2 regulates capacitive Ca^{2+} entry in neurons and plays a key role in hypoxic neuronal cell death. Sci Signal 2:ra67.

Birnbaumer L (2009) The TRPC class of ion channels: a critical review of their roles in slow, sustained increases in intracellular Ca(2+) concentrations. Annu Rev Pharmacol Toxicol 49:395–426.

Blair NT, Kaczmarek JS, Clapham DE (2009) Intracellular calcium strongly potentiates agonist-activated TRPC5 channels. J Gen Physiol 133:525–546.

Bosch MA, Tonsfeldt KJ, Rønnekleiv OK (2013) mRNA expression of ion channels in GnRH neurons: subtype-specific regulation by 17β-estradiol. Mol Cell Endocrinol 367:85–97.

Brini M, Calì T, Ottolini D, Carafoli E (2014) Neuronal calcium signaling: function and dysfunction. Cell Mol Life Sci 71:2787–2814.

Castellano JM, Tena-Sempere M (2013) Metabolic regulation of kisspeptin. Adv Exp Med Biol 784:363–383.

Clapham DE (2003) TRP channels as cellular sensors. Nature 426:517–524.

Clapham DE, Julius D, Montell C, Schultz G (2005) International union of pharmacology. XLIX. Nomenclature and structure-function relationships of transient receptor potential channels. Pharmacol Rev 57:427–450.

Clarkson J, Han SY, Piet R, McLennan T, Kane GM, Ng J, Porteous RW, Kim JS, Colledge WH, Iremonger KJ, Herbison AE (2017) Definition of the hypothalamic GnRH pulse generator in mice. Proc Natl Acad Sci USA 114:E10216–E10223.

Clegg DJ (2012) Minireview: the year in review of estrogen regulation of metabolism. Mol Endocrinol 26:1957–1960.

Cravo RM, Margatho LO, Osborne-Lawrence S, Donato JJ, Atkin S, Bookout AL, Rovinsky S, Frazão R, Lee CE, Gautron L, Zigman JM, Elias CF (2011) Characterization of Kiss1 neurons using transgenic mouse models. Neuroscience 173:37–56.

Czaja JA (1978) Ovarian influences on primate food intake: assessment of progesterone actions. Physiol Behav 21:923–928.

d'Anglemont de Tassigny X, Fagg LA, Dixon JPC, Day K, Leitch HG, Hendrick AG, Zahn D, Franceschini I, Caraty A, Carlton MBL, Aparicio SAJR, Colledge WH (2007) Hypogonadotropic hypogonadism in mice lacking a functional KiSS 1 gene. Proc Natl Acad Sci USA 104:10714–10719.

de Croft S, Boehm U, Herbison AE (2013) Neurokinin B activates arcuate kisspeptin neurons through multiple tachykinin receptors in the male mouse. Endocrinology 154:2750–2760.

De Roux N, Genin E, Carel J-C, Matsuda F, Chaussain JL, Milgrom E (2003) Hypogonadotropic hypogonadism due to loss of function of the KiSS 1-derived peptide receptor GPR54. Proc Natl Acad Sci USA 100:10972–10976.

Dudek M, Ziarniak K, Cateau M-L, Dufourny L, Sliwowska JH (2019) Diabetes type 2 and kisspeptin: central and peripheral sex-specific actions. Trends Endocrinol Metab 30:833–843.

Faber ES, Sedlak P, Vidovic M, Sah P (2006) Synaptic activation of transient receptor potential channels by metabotropic glutamate receptors in the lateral amygdala. Neuroscience 137:781–794.

Gao Y, Yao T, Deng Z, Sohn JW, Sun J, Huang Y, Kong X, Yu KJ, Wang RT, Chen H, Guo H, Yan J, Cunningham KA, Chang Y, Liu T, Williams KW (2017) TrpC5 mediates acute leptin and serotonin effects via Pomc neurons. Cell Rep 18:583–592.

Goodman RL, Lehman MN, Smith JT, Coolen LM, de Oliveira CVR, Jafarzadehshirazi MR, Pereira A, Iqbal J, Caraty A, Ciofi P, Clarke IJ (2007) Kisspeptin neurons in the arcuate nucleus of the ewe express both dynorphin A and neurokinin B. Endocrinology 148:5752–5760.

Gruszczynska-Biegala J, Pomorski P, Wisniewska MB, Kuznicki J (2011) Differential roles for STIM1 and STIM2 in store-operated calcium entry in rat neurons. PLoS One 6:e19285.

Guner G, Guzelsoy G, Isleyen FS, Sahin GS, Akkaya C, Bayam E, Kotan EI, Kabakcioglu A, Ince-Dunn G (2017) NEUROD2 regulates Stim1 expression and store-operated calcium entry in cortical neurons. eNeuro 4: ENEURO.0255-0216.2017.

Han SK, Gottsch ML, Lee KJ, Popa SM, Smith JT, Jakawich SK, Clifton DK, Steiner RA, Herbison AE (2005) Activation of gonadotropin-releasing hormone neurons by kisspeptin as a neuroendocrine switch for the onset of puberty. J Neurosci 25:11349–11356.

Hartmann J, Karl RM, Alexander RP, Adelsberger H, Brill MS, Rühlmann C, Ansel A, Sakimura K, Baba Y, Kurosaki T, Misgeld T, Konnerth A (2014) STIM1 controls neuronal Ca^{2+} signaling, mGluR1-dependent synaptic transmission, and cerebellar motor behavior. Neuron 82:635–644.

Just S, Chenard BL, Ceci A, Strassmaier T, Chong JA, Blair NT, Gallaschun RJ, Del Camino D, Cantin S, D'Amours M, Eickmeier C, Fanger CM, Hecker C, Hessler DP, Hengerer B, Kroker KS, Malekiani S, Mihalek R, McLaughlin J, Rast G, et al. (2018) Treatment with HC-070, a potent inhibitor of TRPC4 and TRPC5, leads to anxiolytic and antidepressant effects in mice. PLoS One 13:e0191225.

Kelly MJ, Rønnekleiv OK (2012) Membrane-initiated actions of estradiol that regulate reproduction, energy balance and body temperature. Front Neuroendocrinol 33:376–387.

Kelly MJ, Qiu J, Rønnekleiv OK (2018) TRPCing around the hypothalamus. Front Neuroendocrinol 51:116–124.

Kuohung W, Kaiser UB (2006) GPR54 and KiSS-1: role in the regulation of puberty and reproduction. Rev Endocr Metab Disord 7:257–263.

Lehman MN, Coolen LM, Goodman RL (2010) Minireview: kisspeptin/neurokinin B/dynorphin (KNDy) cells of the arcuate nucleus: a central node in the control of gonadotropin-releasing hormone secretion. Endocrinology 151:3479–3489.

Livak KJ, Schmittgen TD (2001) Analysis of relative gene expression data using real-time quantitative PCR and the 2(−delta delta CT) method. Methods 25:402–408.

Madisen L, Mao T, Koch H, Zhuo JM, Berenyi A, Fujisawa S, Hsu YWA, Garcia AJ, Gu X, Zanella S, Kidney J, Gu H, Mao Y, Hooks BM, Boyden ES, Buzsáki G, Ramirez JM, Jones AR, Svoboda K, Han X, et al. (2012) A toolbox of Cre-dependent optogenetic transgenic mice for light-induced activation and silencing. Nat Neurosci 15:793–802.

Mayer C, Acosta-Martinez M, Dubois SL, Wolfe A, Radovick S, Boehm U, Levine JE (2010) Timing and completion of puberty in female mice depend on estrogen receptor α-signaling in kisspeptin neurons. Proc Natl Acad Sci USA 107:22693–22698.

Moccia F, Zuccolo E, Soda T, Tanzi F, Guerra G, Mapelli L, Lodola F, D'Angelo E (2015) Stim and Orai proteins in neuronal Ca(2+) signaling and excitability. Front Cell Neurosci 9:153.

Nagae M, Uenoyama Y, Okamoto S, Tsuchida H, Ikegami K, Goto T, Majarune S, Nakamura S, Sanbo M, Hirabayashi M, Kobayashi K, Inoue N, Tsukamura H (2021) Direct evidence that KNDy neurons maintain gonadotropin pulses and folliculogenesis as the GnRH pulse generator. Proc Natl Acad Sci USA 118:e2009156118.

Navarro VM (2020) Metabolic regulation of kisspeptin — the link between energy balance and reproduction. Nat Rev Endocrinol 16:407–420.

Navarro VM, Gottsch ML, Chavkin C, Okamura H, Clifton DK, Steiner RA (2009) Regulation of gonadotropin-releasing hormone secretion by kisspeptin/dynorphin/neurokinin B neurons in the arcuate nucleus of the mouse. J Neurosci 29:11859–11866.

Navarro VM, Castellano JM, McConkey SM, Pineda R, Ruiz-Pino F, Pinilla L, Clifton DK, Tena-Sempere M, Steiner RA (2011) Interactions between kisspeptin and neurokinin B in the control of GnRH secretion in the female rat. Am J Physiol Endocrinol Metab 300:E202–E210.

Nestor CC, Kelly MJ, Rønnekleiv OK (2014) Cross-talk between reproduction and energy homeostasis: central impact of estrogens, leptin and kisspeptin signaling. Horm Mol Biol Clin Investig 17:109–128.

Nestor CC, Qiu J, Padilla SL, Zhang C, Bosch MA, Fan W, Aicher SA, Palmiter RD, Rønnekleiv OK, Kelly MJ (2016) Optogenetic stimulation of arcuate nucleus Kiss1 neurons reveals a steroid-dependent glutamatergic input to POMC and AgRP neurons in male mice. Mol Endocrinol 30:630–644.

Nguyen N, Biet M, Simard E, Béliveau E, Francoeur N, Guillemette G, Dumaine R, Grandbois M, Boulay G (2013) STIM1 participates in the contractile rhythmicity of HL-1 cells by moderating T-type Ca(2+) channel activity. Biochimica et Biophysica Acta 1833:1294–1303.

Niswender CM, Conn PJ (2010) Metabotropic glutamate receptors: physiology, pharmacology, and disease. Annu Rev Pharmacol Toxicol 50:295–322.

Oh-hora M, Yamashita M, Hogan PG, Sharma S, Lamperti E, Chung W, Prakriya M, Feske S, Rao A (2008) Dual functions for the endoplasmic reticulum calcium sensors STIM1 and STIM2 in T cell activation and tolerance. Nat Immunol 9:432–443.

Okamura H, Tsukamura H, Ohkura S, Uenoyama Y, Wakabayashi Y, Maeda K (2013) Kisspeptin and GnRH pulse generation. Adv Exp Med Biol 784:297–323.

Padilla SL, Johnson CW, Barker FD, Patterson MA, Palmiter RD (2018) A neural circuit underlying the generation of hot flushes. Cell Rep 24:271–277.

Park CY, Shcheglovitov A, Dolmetsch R (2010) The CRAC channel activator STIM1 binds and inhibits L-type voltage-gated calcium channels. Science 330:101–105.

Pavez M, Thompson AC, Arnott HJ, Mitchell CB, D'Atri I, Don EK, Chilton JK, Scott EK, Lin JY, Young KM, Gasperini RJ, Foa L (2019) STIM1 is required for remodeling of the endoplasmic reticulum and microtubule cytoskeleton in steering growth cones. J Neurosci 39:5095–5114.

Perissinotti PP, Martínez-Hernández E, Piedras-Rentería ES (2021) TRPC1/5-Cav3 complex mediates leptin-induced excitability in hypothalamic neurons. Front Neurosci 15:679078.

Pfaffl MW (2001) A new mathematical model for relative quantification in real-time RT-PCR. Nucleic Acids Res 29:e45.

Pielecka-Fortuna J, Chu Z, Moenter SM (2008) Kisspeptin acts directly and indirectly to increase gonadotropin-releasing hormone neuron activity and its effects are modulated by estradiol. Endocrinology 149:1979–1986.

Qiu J, Bosch MA, Tobias SC, Grandy DK, Scanlan TS, Rønnekleiv OK, Kelly MJ (2003) Rapid signaling of estrogen in hypothalamic neurons involves a novel G-protein-coupled estrogen receptor that activates protein kinase C. J Neurosci 23:9529–9540.

Qiu J, Bosch MA, Tobias SC, Krust A, Graham S, Murphy S, Korach KS, Chambon P, Scanlan TS, Rønnekleiv OK, Kelly MJ (2006) A G-protein-coupled estrogen receptor is involved in hypothalamic control of energy homeostasis. J Neurosci 26:5649–5655.

Qiu J, Fang Y, Rønnekleiv OK, Kelly MJ (2010) Leptin excites proopiomelanocortin neurons via activation of TRPC channels. J Neurosci 30:1560–1565.

Qiu J, Fang Y, Bosch MA, Rønnekleiv OK, Kelly MJ (2011) Guinea pig kisspeptin neurons are depolarized by leptin via activation of TRPC channels. Endocrinology 152:1503–1514.

Qiu J, Zhang C, Borgquist A, Nestor CC, Smith AW, Bosch MA, Ku S, Wagner EJ, Rønnekleiv OK, Kelly MJ (2014) Insulin excites anorexigenic proopiomelanocortin neurons via activation of canonical transient receptor potential channels. Cell Metab 19:682–693.

Qiu J, Nestor CC, Zhang C, Padilla SL, Palmiter RD, Kelly MJ, Rønnekleiv OK (2016) High-frequency stimulation-induced peptide release synchronizes arcuate kisspeptin neurons and excites GnRH neurons. Elife 5:e16246.

Qiu J, Rivera HM, Bosch MA, Padilla SL, Stincic TL, Palmiter RD, Kelly MJ, Rønnekleiv OK (2018a) Estrogenic-dependent glutamatergic neurotransmission from kisspeptin neurons governs feeding circuits in females. Elife 7:e35656.

Qiu J, Bosch MA, Meza C, Navarro UV, Nestor CC, Wagner EJ, Rønnekleiv OK, Kelly MJ (2018b) Estradiol protects proopiomelanocortin neurons against insulin resistance. Endocrinology 159:647–664.

Roepke TA, Bosch MA, Rick EA, Lee B, Wagner EJ, Seidlova-Wuttke D, Wuttke W, Scanlan TS, Rønnekleiv OK, Kelly MJ (2010) Contribution of a membrane estrogen receptor to the estrogenic regulation of body temperature and energy homeostasis. Endocrinology 151:4926–4937.

Rønnekleiv OK, Qiu J, Kelly MJ (2019) Arcuate kisspeptin neurons coordinate reproductive activities with metabolism. Semin Reprod Med 37:131–140.

Ruka KA, Burger LL, Moenter SM (2013) Regulation of arcuate neurons coexpressing kisspeptin, neurokinin B, and dynorphin by modulators of neurokinin 3 and κ-opioid receptors in adult male mice. Endocrinology 154:2761–2771.

Ryu C, Jang DC, Jung D, Kim YG, Shim HG, Ryu HH, Lee YS, Linden DJ, Worley PF, Kim SJ (2017) STIM1 regulates somatic Ca^{2+} signals and intrinsic firing properties of cerebellar Purkinje neurons. J Neurosci 37:8876–8894.

Salido GM, Jardín I, Rosado JA (2011) The TRPC ion channels: association with Orai1 and STIM1 proteins and participation in capacitative and non-capacitative calcium entry. Adv Exp Med Biol 704:413–433.

Seminara SB, Messager S, Chatzidaki EE, Thresher RR, Acierno JS, Shagoury JK, Bo-Abbas Y, Kuohung W, Schwinof KM, Hendrick AG, Zahn D, Dixon J, Kaiser UB, Slaugenhaupt SA, Gusella JF, O'Rahilly S, Carlton MBL, Crowley WF, Aparicio SAJR, Colledge WH (2003) The GPR54 gene as a regulator of puberty. N Engl J Med 349:1614–1627.

Smith AW, Bosch MA, Wagner EJ, Rønnekleiv OK, Kelly MJ (2013) The membrane estrogen receptor ligand STX rapidly enhances GABAergic signaling in NPY/AgRP neurons: role in mediating the anorexigenic effects of 17β-estradiol. Am J Physiol Endocrinol Metab 305:E632–E640.

Somasundaram A, Shum AK, McBride HJ, Kessler JA, Feske S, Miller RJ, Prakriya M (2014) Store-operated CRAC channels regulate gene expression and proliferation in neural progenitor cells. J Neurosci 34:9107–9123.

Song WJ, Mondal P, Wolfe A, Alonso LC, Stamateris R, Ong BW, Lim OC, Yang KS, Radovick S, Novaira HJ, Farber EA, Farber CR, Turner SD, Hussain MA (2014) Glucagon regulates hepatic kisspeptin to impair insulin secretion. Cell Metab 19:667–681.

Sun Y, Zhang H, Selvaraj S, Sukumaran P, Lei S, Birnbaumer L, Singh BB (2017) Inhibition of L-Type Ca^{2+} channels by TRPC1-STIM1 complex is essential for the protection of dopaminergic neurons. J Neurosci 37:3364–3377.

Tolson KP, Garcia C, Yen S, Simonds S, Stefanidis A, Lawrence A, Smith JT, Kauffman AS (2014) Impaired kisspeptin signaling decreases metabolism and promotes glucose intolerance and obesity. J Clin Invest 124:3075–3079.

Tolson KP, Marooki N, Wolfe A, Smith JT, Kauffman AS (2019) Cre/lox generation of a novel whole-body Kiss1r KO mouse line recapitulates a hypogonadal, obese, and metabolically-impaired phenotype. Mol Cell Endocrinol 498:110559.

Topaloglu AK, Tello JA, Kotan LD, Ozbek MN, Yilmaz MB, Erdogan S, Gurbuz F, Temiz F, Millar RP, Yuksel B (2012) Inactivating KISS1 mutation and hypogonadotropic hypogonadism. N Engl J Med 366:629–635.

Tozzi A, Bengtson CP, Longone P, Carignani C, Fusco FR, Bernardi G, Mercuri NB (2003) Involvement of transient receptor potential-like channels in responses to mGluR-I activation in midbrain dopamine neurons. Eur J Neurosci 18:2133–2145.

Venkatachalam K, Montell C (2007) TRP channels. Annu Rev Biochem 76:387–417.

Wang L, DeFazio RA, Moenter SM (2016) Excitability and burst generation of AVPV kisspeptin neurons are regulated by the estrous cycle via multiple conductances modulated by estradiol action. eNeuro 3:ENEURO.0094-16.2016.

Wang Y, Deng X, Mancarella S, Hendron E, Eguchi S, Soboloff J, Tang XD, Gill DL (2010) The calcium store sensor, STIM1, reciprocally controls Orai and $Ca_V1.2$ channels. Science 330:105–109.

Yuan JP, Zeng W, Huang GN, Worley PF, Muallem S (2007) STIM1 heteromultimerizes TRPC channels to determine their function as store-operated channels. Nat Cell Biol 9:636–645.

Zhang C, Roepke TA, Kelly MJ, Rønnekleiv OK (2008) Kisspeptin depolarizes gonadotropin-releasing hormone neurons through activation of TRPC-like cationic channels. J Neurosci 28:4423–4434.

Zhang Z, Reboreda A, Alonso A, Barker PA, Séguéla P (2011) TRPC channels underlie cholinergic plateau potentials and persistent activity in entorhinal cortex. Hippocampus 21:386–397.

Zhang C, Bosch MA, Rønnekleiv OK, Kelly MJ (2013a) Kisspeptin activation of TRPC4 channels in female GnRH neurons requires PIP_2 depletion and cSrc kinase activation. Endocrinology 154:2772–2783.

Zhang C, Tonsfeldt KJ, Qiu J, Bosch MA, Kobayashi K, Steiner RA, Kelly MJ, Rønnekleiv OK (2013b) Molecular mechanisms that drive estradiol-dependent burst firing of Kiss1 neurons in the rostral periventricular preoptic area. Am J Physiol Endocrinol Metab 305:E1384–E1397.

Zylberberg J, Strowbridge BW (2017) Mechanisms of persistent activity in cortical circuits: possible neural substrates for working memory. Annu Rev Neurosci 40:603–627.